

AD-787 427

FRACTURE IN A TENSILE SPECIMEN

Joseph I. Bluhm, et al

Army Materials Research Agency
Watertown, Massachusetts

July 1966

DISTRIBUTED BY:

NTIS

National Technical Information Service
U. S. DEPARTMENT OF COMMERCE
5285 Port Royal Road, Springfield Va. 22151



AMRA MS 66-06

AMRA MS 66-06

AD 787427

FRACTURE IN A TENSILE SPECIMEN

MONOGRAPH SERIES

by

JOSEPH I. OLUNN

and

ROBERT J. MORRISSEY

JULY 1966

Reproduced by
NATIONAL TECHNICAL
INFORMATION SERVICE
U S Department of Commerce
Springfield VA 22151

D D C
RECEIVED
OCT 22 1974
RECEIVED
F

DISTRIBUTION STATEMENT A
Approved for public release
Distribution Unlimited

U. S. ARMY MATERIALS RESEARCH AGENCY
WATERTOWN, MASSACHUSETTS 02172

68

FRACTURE IN A TENSILE SPECIMEN

**Joseph I. Bluhm
and
Robert J. Morrissey**



July 1966

**Presented at
International Conference on Fracture
Sendai, Japan
September 1965**



FRACTURE IN A TENSILE SPECIMEN

Joseph I. Bluhm^[1] and Robert J. Morrissey^[2]

There appears to have been little or no attempt to study the stress or strain conditions under which internal fracture starts and/or propagates in the neck of a tensile specimen. Using a continuous ultrasonic "searching" technique, this "incipient" internal fracturing has been investigated in a variety of low strength ductile metals. Voids of approximately 0.001 inch in size have been signalled ultrasonically and confirmed metallographically. This paper is centered around the evaluation of crack propagation with emphasis on void formation and coalescence and interpretation in terms of a non-adiabatic shear separation process.

INTRODUCTION

The tensile test is perhaps one of the most studied and utilized of mechanical tests for evaluation of materials. Nevertheless, there are still many facets of materials behavior as exemplified by this test which are still ill understood. Even in the matter of ultimate tensile strength and its associated criteria and strains, some clarification is required. Beeuwkes,^[3] for example, has shown that one must distinguish between incipient maximum load and incipient necking - that these are not necessarily the same points on the load-deformation curve - that the strain at maximum load may be appreciably different than the strain at incipient necking.

Certainly the state of stress and strain within the neck is known only to a degree of approximation, as suggested by such investigators as Bridgman,^[4] Skudnov and Sokolov,^[5] or Davidenkov and Spiridonova.^[6] One of the obvious motivations for these latter studies is the determination of

-
1. Chief, Applied Mechanics Research Laboratory, U. S. Army Materials Research Agency, Watertown, Massachusetts 02172, U.S.A.
 2. Mechanical Engineer, U. S. Army Materials Research Agency, Watertown, Massachusetts 02172, U.S.A.
 3. Beeuwkes, R., Personal communication, Watertown Arsenal Laboratories, Watertown, Mass. 1952-1960.
 4. Bridgman, P. W., Transaction of American Society for Metals, Vol. 32, 1944, pp. 553-574.
 5. Skudnov, V. A., and Sokolov, L. D., Industrial Laboratory, Vol. 30, No. 9, September 1964, pp. 1388-1390.
 6. Davidenkov, N. N., and Spiridonova, N. I., Proceedings of ASTM, Vol. 46, 1946, pp. 1147-1158.

the stress and/or strain state, for example, in the neck of a specimen so that a more systematic presentation of stress-strain curves can be made in terms of significant effective stresses (or strains) which require the knowledge of all the component stresses (strains). This use of the "neck" stress state has indeed served its purpose; it is commonplace to present effective stress-strain data well into the necking region and, in fact (as we shall later see), too far into the necking region for valid results. A second important and obvious use to which these "neck" results can be applied is for the determination of the stress (strain) state, particularly at incipient fracture. It has been suggested [7,8,9,10] that fracture in smooth ductile specimens initiates generally as minute crack or void formation in the interior of the neck region near the specimen axis. Knowledge of the stress (strain) state within the specimen, therefore, is necessary if one hopes to verify a fracture criterion.

Once cracking, tearing, void formation, or even localized concentration of slip bands has started, then, of course, the idealized neck analysis of the above investigators is invalid and one is left with a condition for which extremely little is known.

Eventually, the cracking and/or tearing proceeds to a point where further deformation of the specimen takes place principally by a gross shearing process leading to separation and the associated well-known shear lip or "cone" of the cup-cone fracture. We shall speculate in this paper that this ultimate shear separation is, in fact, merely a smooth continuation of the earlier flow and necking process which is considered to have been momentarily interrupted by the initiation and propagation of the interior voids or crack; but that when the conditions for continued tearing, i.e., the hydrostatic tension, diminished sufficiently, the flow again proceeds but now under a condition which can be closely approximated by a plane strain in lieu of the more complex rotational symmetric state. Furthermore, our results indicate that separation of the specimen is not necessarily adiabatic but behaves so only from the circumstances of the flexibility of the loading system and specimen.

In the usual tensile test, the quantities generally measured are the yield strength, tensile strength, elongation, and the reduction of area. The first two delineate the onset, at least approximately, of distinct phenomena, "yielding", and "necking", or instability. As already implied above, however, there is at least one additional stress level which should be observed and

7. Plateau, J., Henry, G., and Crussard, C., *Review de Metallurgie*, Vol. 54, 1957, p. 200.
8. Low, J. R., Jr. *Fracture of Solids* - Drucker, D. C., and Gilman, J. J., Editors, Interscience Publishers, 1962, p. 197.
9. Puttick, K. E., *Philosophical Magazine*, Vol. 4, 1959, p. 964. Also Vol. 5, 1960, pp. 759-762.
10. Rogers, H. C., *Fundamental of Deformation Processing*, Syracuse University Press, 1964. Also *Transactions of AIME*, Vol. 218, 1960, p. 498.

recorded, and that is the point at which fracture "first" occurs. Most commonly, this is assumed to be the same as the stress at which the specimen breaks into two pieces, but this generally is far from the truth. For an unnotched and reasonably ductile metal, this initial "fracture" occurs near the longitudinal axis of the specimen in the region of the neck - after the neck has formed but before separation. In a conventional test, deformation continues under continued loading until the specimen breaks rapidly and uncontrollably into two pieces. The load at which this occurs is used to calculate the fracture stress. The true local stress at initial or incipient fracture generally is considerably different than the stress at rapid separation, particularly in ductile specimens. The final stages of specimen separation take place generally by formation of shear lips as distinct from the more flat internal fracture. A specially-designed rigid device permitted the present investigators to control this entire separation stage in several materials which normally failed rapidly and without control.

The percentage reduction of area (% R.A.) is a measure commonly made and generally based upon the initial and final diameter. It has become not uncommon currently to recognize the distinction between the uniform R.A. and that associated with localized necking. In view of the occurrence of internal fracture, appreciably in advance of final separation, one might indeed inquire into the real significance of an R.A. referred to the post separation areas. This point is discussed in detail in the main text.

In the usual tensile test, the stiffness of the specimen and testing machine is very low, and rapid disruption of the specimen results at some point in the test. This condition for rapid ductile fracture was shown by Orowan^[11] to be governed by the relation

$$\frac{d^2W}{dx^2} = - \frac{d^2U}{dx^2}$$

where

U = elastic energy of the specimen

W = plastic work required for next contraction during an increment dx of plastic extension.

This relationship is equivalent to specifying that rapid necking occurs when the slope of the plastic load deformation curve is the same (except for sign) as the gradient of elastic load deformation release lines. At point P of Fig. 1, for instance, a virtual plastic displacement would result in the load dropping more rapidly than the force required for further yielding; so that the condition at P is stable until further extension is enforced. At point Q, the specimen is unstable. Any further extension leads to a situation where the elastic force drops off less slowly than the force required for further yielding; hence, rapid necking proceeds at the expense of the stored elastic energy in the specimen and/or testing machine. This is the so-called elastic-plastic instability which Orowan calls high velocity ductile fracture. With a "stiffer" tensile tester, the elastic load release line will tend toward the vertical, and rapid ductile fractures will tend to occur

11. Orowan, E., Journal of Applied Physics, Vol. 26, July 1955, pp. 900-902.

further to the right of point M (i.e., at greater extension). In fact, rapid ductile fracture may be virtually suppressed completely with a sufficiently rigid machine.

It should be quite apparent by now that in spite of the long history of the "straightforward" and "simple" tensile test, a great deal is still unknown so far as the significance of some of the properties measured therefrom. It is hoped that the present study will throw some light on some of the aforementioned considerations.

MATERIALS

Except for a few preliminary tests conducted on an initial small batch of copper Cu-I, some SAE 4340 steel, and some SAE 1026 steel, the principal test program was centered about a second batch of commercially-pure copper Cu-II and an SAE 1020 and SAE 8620 steel. The composition and conventional mechanical properties are given in Tables I and II respectively. The form and/or condition of the materials as used are as follows:

- Copper I - one length of 1 inch diameter cold drawn rod.
- SAE 1026 steel - one length of 1 inch diameter cold rolled rod, as received (annealed).
- SAE 4340 steel - one length of 3/4 inch diameter cold rolled rod, heat treated to $R_c = 41$.

(Specimens taken from the above three materials were machined concentric with the bar stock axis).

- Copper II - one length of 2 inch diameter cold drawn rod; specimens machined symmetrically (four to a cross-section) on a 1-3/16 inch diameter.
- SAE 1020 steel - one length of 2-3/4 inch diameter rod, as received (annealed); specimens machined symmetrically (six to a cross-section) on a 1-7/8 inch diameter.
- SAE 8620 steel Grade CEVME - one length of 2 inch diameter rod; specimens machined symmetrically (four to a cross-section) on a 1-1/4 inch diameter as received.

Microphotographs of the Cu-II, SAE 1020, and 8620 in the virgin, i.e., unstrained state, are shown in Fig. 2, ^[12] 3, and 4, respectively.

TESTING PROCEDURE

In order to investigate the initiation and growth of the fracture path including the stage of shear lip formation, it was necessary to develop a reasonably stiff "tensile testing machine". Starting with a design after McClintock, et al, ^[13] several major modifications were incorporated; these were principally for the purpose of (a) facilitating continuous loading;

12. The scale and/or magnifications shown in all microstructures apply before reduction for reproduction.
13. McClintock, F., Alpaugh, H., Dougel, S., and Kuebler, M., Massachusetts Institute of Technology, Research Memorandum No. 38, 1962. (unpublished)

- (b) preventing the possibility of transmitting torsion to the specimen; and
- (c) accommodating an ultrasonic crystal as a crack detecting system.

The Rigid AMRA Tester (RAT) enabled the investigators to maintain complete control over crack growth throughout all stages of fracture in smooth tensile specimens of ductile materials and control in the earlier stages of the fracture of more brittle materials. Some further refining is desirable to permit control in high-strength brittle materials of the later stages of crack growth.

A schematic representation of the RAT assembly is shown in Fig. 5 and an exploded view in Fig. 6. Specimens of 0.252 inch diameter were consistently used. Other pertinent dimensions of the specimen are shown in Fig. 7.

The specimen is assembled in the RAT and set up in a tensile testing machine. A load of approximately 100 pounds [4] is applied with the tensile tester [5] to permit rotation of the collar (via the collar spokes) without rotating the grips of the tensile testing machine. Relative rotation of the collar on the threads engaging it to the collar grip determines the width of the gap between the lower bearing plate and the internal face of the collar.

The extent to which the specimen may elongate, hence, the extent to which plastic deformation including necking and/or internal fracture may occur after the maximum load is reached, is governed by the width of this gap. Increments of specimen elongation (increments of gap width) are measured by the extent of the rotation of the collar beneath the thread advance indicator. The collar surface that the indicator is pressed against has radial graduations engraved on it at 10 degree intervals which corresponds to 0.002 inch [6] of specimen elongation. Elongation can be controlled in increments of about 0.0005 inch [6] provided the applied load of the tensile tester does not exceed the load on the specimen by more than several hundred pounds.

When the RAT is set up in a tensile tester with the 100 pound preload applied, the gap is widened to a sufficient width to allow the specimen to elongate to maximum load. At maximum load, the RAT is bottomed (gap width = 0) and the applied load of the testing machine is increased several hundred pounds, which goes almost entirely to elastically deform the collar a small amount.

Rotating the collar a small amount (in the direction tending to open the gap) will allow the specimen to elongate slightly and cause a reduction in the hitherto constant applied load of the testing machine. The applied load

14. This requirement can be simply eliminated by merely torsionally clamping the specimen grips to any convenient fixed reference point.
15. Henceforth, in the present text, "tensile machine" or "tensile tester" will refer to a typical tensile testing machine; whereas, RAT will refer to the device which is used in conjunction with a tensile testing machine in order to enhance the effective stiffness of the tensile testing machine.
16. These can be refined readily by changing the thread to a finer pitch.

is again increased to several hundred pounds greater than the load on the specimen before the second rotation of the collar. By this procedure, the gap is kept closed and rotation of the collar merely permits a controlled deformation of the specimen to take place.

Repetition of this above incremental elongation procedure allows complete control of crack growth throughout all stages of fracture in the more ductile materials and in the earlier stages of fracture of brittle materials. The splined coupling prevents the transmission of torque through a partially fractured specimen as the collar is rotated.

The load on the specimen, which is equal to the applied load of the tensile tester only when the gap in the RAT is not zero, is recorded on a strain indicator connected to a load cell in series with the specimen.

In addition to mechanically controlling the deformation of the specimen, a 1/4-inch-diameter, 5 megacycle quartz crystal ultrasonic transducer mounted on the end of the specimen was used to continuously "search" the specimen for signs of the initial internal crack appearance.

Photographs of typical ultrasonic response signals (pulse-echo technique) at various load stages are shown in Fig. 8 and 9 for Copper Cu-I and SAE 4340 steel, respectively. These figures show two large "pips", the input pulse on the left and the back echo on the right. The pip at the left center is a specimen shoulder echo. Pips indicating fracture appear at right center. The multiple "crack pips" (see Fig. 8c) are thought to be due to the irregular reflecting surface of the fracture. A loss in the amplitude of the recorded signal as deformation increased (indicated by the relative height of the back echo "pip") can be noted by comparison of these photographs. This appears to be attributable to both the presence of attenuation resulting from plastic flow and the formation of the fracture.

Metallographic observations were made to verify the ultrasonic techniques and to determine crack profile, the relationship of grain structure, and crack orientation.

Initially, the metallographic searching procedure consisted of grinding the mounted specimen parallel to its axis and polishing and examining them microscopically at several depths approximately 0.010 inch apart near the axis. This crude technique proved to be inadequate in attempting to verify the earlier stages of fracture where the predominant fractures were considerably smaller than 0.010 inch and, in many instances, originated at radial distances relatively remote from the axis. Consequently, specimens were mounted and ground to a distance of approximately 0.4 of the radius from the axis and then examined at depth intervals of 0.002 to 0.003 inch. These incremental removals of material were accomplished by merely repeating the final steps of the normal polishing procedure.

RESULTS AND DISCUSSION

General

Some six materials, as indicated in Tables I and II, were examined in all. These were tested in simple tension in either a conventional Timius Olsen 120,000 pound hydraulic unit alone or in conjunction with the Rigid AMRA Tester.

Limited preliminary and exploratory tests only were conducted on the copper Cu-I, and the SAE 1026 and SAE 4340 steels. These tests were aimed principally at (a) verifying the suitability of the ultrasonic crack detection techniques; (b) checking the operation of the RAT; (c) exploring the metallographic search techniques; and (d) selecting materials suitable for testing in the present RAT.

Typical load deformation curves for these three preliminary materials are shown in Fig. 10. Isolated specimens of the copper Cu-I and the SAE 1026 steel were pulled (in the RAT) to the points, beyond the knee, indicated with the circles and subsequently metallographically searched for cracks. The test of an SAE 4340 steel specimen was stopped somewhat sooner, as shown, and also metallographically examined.

Fig. 11, 12, 13, and 14 show the cursory results of these metallographic searches. The copper specimen (Fig. 11), pulled well beyond the knee, displayed a well opened-up crack and was almost completely separated with only a small edge annulus still maintaining the specimen intact. In fact, the final shear separation was actually visible at some points on the periphery, as evident in Fig. 12. During the testing of this specimen, the load was controllably reduced (as the specimen continued to extend) from a maximum of 2340 pounds to 190 pounds in the RAT, at which time the loading was intentionally stopped to preserve some of the peripheral shear band without final complete shear separation. The SAE 1026 steel specimen, however, was pulled only slightly beyond the knee and displayed the somewhat shorter and relatively unopened crack visible in Fig. 13.

In the case of the tests of the SAE 4340 steel specimens, it was found to be almost impossible to prevent completion of the separation stage. Generally shortly after, but almost simultaneous with the first echo pulse, final fracture and separation would occur even when tested in the RAT. Nevertheless, in at least one instance of the SAE 4340 material (Fig. 10), it was possible, by the use of the RAT, to stop the test just after the first echo pulse (see Fig. 9) but before uncontrolled fracture occurred. Fig. 14 shows the crack found in this specimen by subsequent metallographical searching by successive polishing procedures which incrementally removed some 0.012 to 0.017 inches. It is, therefore, likely that the crack seen in Fig. 14 did not necessarily reflect the maximum possible size of the crack which existed. Nevertheless, the observed crack of the order of 0.002 to 0.003 inch emanating from a central "void" provided some preliminary insight to the size of defect the ultrasonic search technique was able to detect. For examination of subsequent specimens, the surface was ground off in successive 0.002 to 0.003-inch layers polished, etched, and examined metallographically at each increment in order not to miss the first evidence of voids and/or cracks, i.e., the incipient void or crack formation condition.

All subsequent tests were conducted on a second batch of copper, i.e., Cu-II, SAE 1020 and SAE 8620 steel. Of this group, a number of the specimens were pulled either conventionally as before or in the RAT with or without ultrasonic search equipment to selected predetermined points on the load-deformation curves intermediate between the incipient fracture point and the point at which final separation of the specimen was complete. A composite load-deformation curve for the series of copper Cu-II specimens identifying a number of, and the scatter of, the critical points is shown in Fig. 15. Fig. 16 reveals the progress of the failure within the neck at various points along

this curve and, finally, Fig. 17 is the corresponding true stress-true strain curve. Fig. 18, 19, and 20 relate similarly to the SAE 1020 steel specimens and Fig. 21, 22, and 23 relate to the SAE 8620 steel specimens.

Rather than presenting or plotting the curves for all specimens tested, a typical representative curve is shown for each material and when more than one curve was obtained, then the individual points corresponding to critical points for the other specimens of the same material were superposed on the curve. Since curves of duplicate specimens for a given material were essentially identical up to the point of detection of incipient fracture, the curve shown represents the typical behavior to this point. The additional notations for individual specimens at incipient fracture and at incipient shear are self-explanatory. The apparent scatter in location of critical points stems from the slightly different total elongation of the different specimens. The final "drop off" in load normally observed and identified in Fig. 15, 18, and 21, with the notation "uncontrolled separation", corresponds to uncontrolled rapid ductile fracture and is associated with the use of a "soft" testing machine. On the other hand, the "drop off" shown in the solid line was obtained by the use of the RAT and corresponds to a slow well-controlled fracture and/or shear separation. This will be discussed more fully later.

Detailed summary data corresponding to the measurements and computation at the following critical points along the load-deformation curve are tabulated in Tables III, IV, and V.

- | | |
|---|---------------------|
| a. Initial state, | d. Incipient shear, |
| b. Incipient necking, | e. Final state. |
| c. Incipient fracture
(void and/or crack formation), | |

Here a. and e. refer merely to the initial shape and final shape (after separation) of the specimen respectively, and b. refers to the condition at necking.

Detailed discussion of the tests, observations, and data outlined above are given in the following sections, particularly with respect to incipient fracture and incipient shear separation.

Incipient Fracture (Void or Crack Formation)

The point of incipient fracture (void or crack formation) was determined using the ultrasonic search technique described earlier and was taken as the point at which a first echo pulse was observed in the recording oscilloscope. It was expected that this initial cracking would occur within the neck of the specimen. Accordingly, it was possible to anticipate approximately where this echo pulse would appear in the observed trace, thus facilitating its identification provided, of course, the echo was a direct reflection from the crack and not an indirect bounced reflection as one might expect from the surface of a crack inclined to the axis of the specimen. In order to be reasonably certain that the echo pulses were indeed indicative of the presence of a crack, several of the preliminary specimens were X-rayed at various stages of deformation beyond the occurrence of the first echo; but because of the limited sensitivity of this method, cracks were "visible" only after an appreciably greater deformation and crack extension than that at which the first echo

pulse was observed. Nevertheless, X-rays did serve to substantiate the presence of gross cracks at greater deformations. Earlier detection and/or confirmation was, however, desired; therefore, several specimens were selected in which the testing had been terminated just as an echo pulse had just been observed. These were deformed slightly additionally to accent the crack and then metallographically "searched".

Fig. 24, 25, 26, 27, 28, and 29 show the results of subsequent similar surveys on the copper Cu-II, SAE 1020, and SAE 8620 materials respectively deformed to just before the final knee. It will be observed that rather than having a well-defined single void and/or crack as could be anticipated, there appears to be a small domain in the neck region in which a number of small voids and/or microcracks are concentrated. In no specimen was a large well-defined single crack observed; rather, a domain of multiple tiny cracks or voids was evident. This latter observation is consistent with those of Rogers. [10] In the copper specimen (Fig. 24 and 25), the void formation is highly oriented in the longitudinal direction; whereas, this preferred orientation was not evident in either of the other two materials (Fig. 26 and 27 or Fig. 28 and 29). From other tests of specimens not extended quite so far but rather to only slightly beyond the first ultrasonic echo pulse, it was evident that the void or microcrack domain initiated approximately at the echo point and expanded under continued deformation. From these examinations, it was further evident that the point of incipient fracture, like the true yield strength of a metal, depends upon the sensitivity of the detection system, either ultrasonically or metallographically. Undoubtedly, initial void formation or cracking occurred somewhat sooner than when we were able to detect it. Nevertheless, no further significant effort was made to further define incipient fracture beyond the acceptance of a reasonably evident indication from our ultrasonic search system. It was possible to get somewhat earlier detection by increasing the sensitivity of the amplifiers, but this also introduced considerable "noise" and made certain detection somewhat more doubtful. Based, however, upon the overall limited experiences reported, it is estimated that voids and/or cracks of the order of 0.001 inch could be defined with a high degree of certainty and that defects appreciably smaller than this were undoubtedly being detected.

Occasionally, either no indication of a crack became evident till very late in the load history, or the critical indication suggested a crack much further from the detection crystal than the neck. This was attributed to the initial development of the void or crack in an oblique orientation as, for example, in a conical surface (the volcano configuration) which could cause the reflecting echo to take a long path back to the crystal thus creating the illusion of a somewhat more distant void or crack.

Nevertheless, for most of the specimens, a sharp indication was observed and was reasonably reproducible from specimen to specimen. Based upon the result of these well-behaved specimens, incipient "fracture" was well defined. At this apparent incipient fracture point in the load deformation curve, measurements were made of the load, the minimum cross-sectional diameter of the necked section, and the neck profile radius. Calculations were made using the Bridgman analysis [4] for the stress distribution in the neck. Fig. 30 shows typical stress results - note the rather shallow drop off in longitudinal stresses from the peak center value as the radial distance increases. The gentle drop off in this stress distribution (approximately 20 percent) undoubtedly accounts for some of the off-center voids and cracks and for the finite

domain inhabited by these early voids - particularly noticeable in Fig. 24 and 28. The difference in the peak longitudinal stress at the axis and at the edge of the specimen is a measure of the hydrostatic tension. The presence of this hydrostatic field contributes prominently to the minute void or crack formation process leading to shear deformations and subsequent fracture which must, therefore, of necessity, be restricted to short range (microscopic) [17] paths.

Rows 13 to 18 inclusive (Tables III to V) summarize the state of stress and strain specifically at the center of the necked region for incipient fracture. These values may be used to calculate the effective stress [18] and effective strain, [18] which will be used later to unify the tensile deformation process. The maximum longitudinal stresses are given in row 15.

Note the comparison below (taken from Tables III, IV, and V) of the relative level of ultimate, incipient fracture, and conventional fracture strengths:

	<u>Copper II</u>	<u>SAE 1020</u>	<u>SAE 8620</u>
Ultimate Strength	42,100	60,400	77,400
Incipient Fracture Strength	67,500	101,500	130,000
Conventional Fracture Strength	73,000	116,500	141,400

Crack Propagation and Incipient Shear

After incipient fracture, i.e., void/crack formation, continued loading of the specimen appears to have the influence of increasing the density of the voids/cracks and expanding the domain populated by them. Eventually, the load-deformation curve undergoes a marked break or "knee" in the curve, and the load drops steeply relative to the deformation (see Fig. 15 and 16, or 18 and 19, or 21 and 22). Metallographic examination of specimens pulled up to this point failed to reveal in any of the specimens examined any signs of a gross (nonmicroscopic) crack and, in fact, showed only regions well populated with microscopic (a) voids, (b) interfacial non-connected cracks at inclusions, or (c) short intercrystalline cracks. As indicated in the previous section, Fig. 24 through 29 show typical appearance of the neck region at or just prior to the knee in the three principal test materials. These metallographic results further show that though the void/crack populated domain is of appreciable size, as observed above, at the knee of the curve there is no evidence of the development of the gross shear lips. Note the absence of any visible alignment of voids or cracks or shear deformation along the potential shear bands.

17. For ideal flawless materials, a sufficiently high, pure hydrostatic tension would lead to cleavage without prior shear deformation. However, for real materials, inherent defects and natural crystalline anisotropy gives rise, even under pure externally applied hydrostatic tension, to local short range shear fields and the consequent possibility of shear flow and fracture on a localized basis.
18. Defined later.

Fig. 31 through 34 inclusive, show the typical microstructure in copper Cu-II and SAE 8620 specimens pulled to a load just beyond the "knee". Although a number of SAE 1020 specimens were tested, no SAE 1020 specimens were photographed in this position; but the results were essentially identical. In almost every case for each of the materials examined, a simple crack or network of microcracks was evident; but it was still not possible to positively identify the onset of the gross shears associated with the ultimate shear lip formation. The void/crack domain size, nevertheless, was appreciably expanded, as is quite evident by comparison of Fig. 28 and 33. However, for specimens pulled further along the load-deformation curve, the operation of lip formation becomes visible and obvious. In fact, for a number of specimens pulled well beyond the knee of the curves, as for the copper Cu-I mentioned earlier (Fig. 10, 11, and 12), the shear lip may be completely developed at some angular positions of the specimen. Fig. 35, 36, and 37 show the corresponding partial shear lip development in specimens of copper Cu-II, SAE 1020, and SAE 8620, respectively. The shear separation is clearly visible on the surface.

More detailed metallographic views of several copper specimens deformed well beyond the "knee" are shown in Fig. 11 and 38 through 45 inclusive. There are revealed in Fig. 11 and Fig. 44 and 45, a considerable number of holes elongated in the direction of the applied load and generally concentrated in the necked region. In the specimen shown in Fig. 11, a surface step formed by radial yielding is noted at the left end of the crack. Two local shear zones form the upper and lower boundaries of the material that yielded radially. Reorientation of the inclusion holes along the shear zone paths can also be observed and is quite evident in Fig. 45, where again a surface step is visible. Here, cavity coalescence appears to be concentrated along the shear zones. Final separation can apparently also take place as a tensile failure, as suggested by Puttick [9] (see, for example, right side of Fig. 11). Here, we note that where the tearing approaches the right surface, the fracture develops between the two shear flow zones. The process by which the fracture spreads toward the specimen surfaces appears to be one of coalescence of inclusion holes which enlarge with straining. It is interesting to note that where the fracture approaches the right surface, the high strain bands, visible along the plane of maximum shear stress, are almost coincident with another at the upper left region.

Gross opening of the void/crack network does not appear to occur in the materials examined until the flow field becomes concentrated into the narrow shear band which eventually develops into the shear lip. Only then do the relatively large shear deformations in these bands lead through the deformation compatibility requirements to the growth of the void into gross cracks which microscopically open up. Fig. 13 shows, for example, the crack detail in an SAE 1026 specimen pulled just beyond the knee; here the cracks have extended, but no significant opening is noticeable nor were there any signs of lip formation. However, tests of the Cu-II, SAE 1020 and SAE 8620 pulled to points well beyond the knee and, in some cases almost to the point of complete separation, showed definite microscopic opening of the crack and, in fact, quite visible shear band formation. Fig. 38 through 41 and Fig. 42 through 45 show the detailed appearance in copper Cu-II specimens of the cracks at (a) an intermediate point between the knee and total separation, and (b)

at almost total separation. Fig. 46 and 47, and 48 and 49 correspond equivalently in the SAE 1020 steel. Fig. 50 and 51 show the unetched details of an SAE 8620 specimen deformed to an intermediate position between the knee and final separation.

The general zig-zag configuration evident in most of these specimens is consistent with the behavior proposed by Rogers.^[10] Rogers has shown that under continued deformation voids form and tend to coalesce to form larger holes. Furthermore, he has suggested that these voids tend to form in sheets at plus or minus 30 to 40 degrees from the longitudinal axis of the specimen, and the subsequent rupture follows one of these alternative paths. The rupture then tends to propagate always back toward the plane of maximum stress in the plane perpendicular to the longitudinal axis; hence, the fracture vacillates amongst these two paths and results in the zig-zag fracture path that one frequently observes. The internal zig-zag steps are relatively short because of the high hydrostatic tension; but as the crack propagates toward the free surfaces, this component diminishes and the last zig is large, forming the so-called shear lip.^[19]

From these numerous observations, both macroscopic as well as microscopic, it appears that the knee is associated with the commencement of the gross shear deformation which eventually culminates in the shear lip. As this gross deformation proceeds, the "porous" domain at the interior of the neck undergoes a period of gross coalescence or expansion of voids, as a result of the required compatibility of deformation of the neck interior and the material playing a part in the shear lip formation.

Assuming then that incipient shear separation is indeed associated with the drop off observed in the load-deformation curve, it is further suggested that this final shear separation is merely a continuation of the earlier flow process which led first to necking and then to incipient cracking or void formation and that this latter process merely interrupted temporarily the flow process. If these are indeed the circumstances under which final shear separation occurs, then it should be possible to construct an effective stress-effective strain curve of the material which should exhibit reasonable continuity through the necking and incipient fracture point as well as the incipient shear separation point. The data reflecting the stresses and strain at this incipient shear separation point are given in Tables III to V. The results of the effective stress-effective strain correlation are discussed later.

-
19. Ideally, if the hydrostatic tension fields persisted as coalescence proceeded, final fracture would, of necessity, be by cleavage and no shear could occur. However, for real materials having defects and crystalline anisotropy, even a pure hydrostatic tension field applied in the center region of the specimen does give rise to local "short range" shear fields with their resultant possibility of shear fracture--but on a localized basis. As the crack or void domain extends toward the free surfaces, the hydrostatic field diminishes until essentially a simple biaxial or uniaxial stress field predominates and gives rise then to a long range shear field and to a final gross shear separation forming the eventual shear lip or "cone" of the typical cup-cone tensile fracture.

It has frequently been suggested that both the "drop in beam" phenomenon, at upper yield, heralding the onset of flow in a tensile specimen, as well as the final shear separation, are adiabatic processes. Indeed, in the usual testing system employing a relatively flexible loading machine, both these occur with such speed as to justify the assumption of adiabaticity. However, the implication that at least the latter of these phenomena must, of necessity, be adiabatic does not appear to be substantiated by our tests. Specimens which consistently failed in a rapid uncontrolled and presumably adiabatic manner when tested conventionally in a "soft" testing machine, behaved ideally when tested in our RAT. Not only was rapid uncontrolled fracture with the accompanying obliteration of the related load-deformation curve avoided, but it was possible to repeatedly start and stop the fracturing process and obtain the entire load-deformation history from incipient shear separation to final complete separation. These tests were conducted at speeds which would appear [20] to assure more nearly isothermal conditions than adiabatic. The curves shown in Fig. 15, 18, and 21 show the result of testing in the RAT; when tested in a conventional tester, the curves dropped abruptly and uncontrollably at the point identified by the notation "uncontrolled separation". This sometimes happened even in the RAT in view of its limited stiffness. A redesign is under-way to stiffen the tester.

Resumé

From our studies, it appears that the fracturing process is related to the load-deformation curve in the following general manner:

a. After "necking" and in the environment of a hydrostatic tension field concentrated in the central region of the "neck", tiny microscopic cracks and/or voids develop at inclusions, crystallographic defects, or grain boundaries (particularly triple points), etc., in much the fashion described by Puttick, [9] Beacham, [21] and Gurland and Plateau. [22] These continue to nucleate expanding over an internal volume presumably governed by the applied load and the shape of the neck--the larger the ratio of the profile radius R to the cross-sectional radius a , i.e., R/a , the larger the volume of void participation in the failure process--the smaller the R/a , the more confined the volume of void

20. Deformation rates step-wise for a given specimen corresponded to a minimum average value of head motion (approximately 1-1/2 inches gage length) of 0.0001 in/min.

21. Beecham, C. D., Transactions of ASM, Vol. 56, 1963, pp. 318-326.

22. Gurland, J., and Plateau, J., Transactions of ASM, Vol. 56, 1963, pp. 442-454.

participation. [23] Under the influence of the hydrostatic tension, short range shear fields predominate and provide the driving force for rupture between voids and/or cracks.

b. Thus, with continued gross extension of the specimen, the void/crack volume expands leaving a matrix weakened by voids/cracks in the center of the neck region and an outer periphery of metal in a substantially unfractured state and in a state of zero or low hydrostatic tension. This final annulus of solid material is, therefore, under a long range shear field and begins to shear in a gross manner in the narrow bands which will delineate the final shear lips. Compatibility of deformation then causes gross coalescence of the central voids to form large macroscopically visible internal cracks which grow as the final shear lips are formed. The matrix network ruptures either by localized necking of ligaments, per Kraft, [24] or by shear, per Edelson et al. [25, 26] This latter gross shear separation is associated with the "knee" of the load-deformation curve.

c. Finally, depending on the relative stiffness of the testing system, the specimens either separate rapidly and approximately adiabatically [27] forming the final shear lips, or the specimens may be controlled so that separation is a slow, essentially isothermal, process. Examination of several specimens of the copper Cu-II and the steels tested in both manners failed to show significant macroscopic differences. The shear lips not only were not suppressed in the controlled tests, but were identical in size and appearance to those obtained by conventional test.

It was earlier suggested that the final shear separation might well be a delayed continuation of the earlier flow and necking process and that if this were indeed the case then within the accuracy of calculation one would expect

-
23. The larger the R/a the more gentle the neck and the less pronounced is the hydrostatic tension influence. Hence, the significant flow stresses would be solely the longitudinal stress which would be essentially uniform and cover a large volumetric domain in which void and/or crack formation could occur. On the other hand, for small R/a, the neck is pronounced and localized; the hydrostatic tension component is significant but restricted to a small volumetric domain within the neck, and void/crack formation would be accordingly restricted.
 24. Kraft, J., presented at ASTM Special Committee on Fracture Testing of High Strength Metals (ASTM-PTHSM), Cleveland, Ohio, 9 September 1964.
 25. Edelson, B., Transactions of ASM, Vol. 56, No. 1, March 1963, pp. 82-89.
 26. Edelson, B., and Baldwin, W., Transactions of ASM, Vol. 55, No. 1, March 1962, pp. 230-250.
 27. The rapid (adiabatic) separation may occur at a point in the load-deformation curve prior to the normal "knee" - its position is governed by a criteria equivalent to that by Orowan (loc cit).

a smooth effective stress-effective strain [28] curve encompassing all the so-called critical points. Accordingly, at the maximum load point, at incipient cracking and at incipient shear separation, the three components of stress and strain were determined (as described below) and then combined to form the effective stresses and effective strains. [28] Fig. 52 shows the results of such a procedure. Here the effective stress-effective strain curve is plotted. Through the point of incipient necking, the analysis of stresses and strains is straightforward. Between necking and incipient cracking, the stresses are determined using the Bridgman procedure; the strains are determined from the measured diameter of the neck and from the assumption of uniform strain distribution across the neck and incompressibility. At the incipient shear point, the stresses were based upon (a) the observed axial load and the corresponding remaining annular cross-section determined by post-facto examination; (b) the assumption of a plane strain condition which permitted an approximate calculation of the hoop stress; and (c) the assumption $\sigma_r = 0$ (since it is zero at outside surface and zero at internal surface of crack or void domain). The strain calculations were based upon the measured diameter, the assumption $\epsilon_r = \epsilon_\theta$, and incompressibility of material. The data for and the results of these computations are indicated in Tables III to V and are plotted as indicated in Fig. 52. Much remains to be desired in concluding that the incipient shear separation point lies on the smooth extension of the effective stress-effective strain curve. Yet, considering the ambiguity of the cross-sectioned area involved and the uncertainty as to the stress and strain levels in the unfailed annular which develops into the shear lip, it does not seem too unreasonable to consider the final shear to be a final phase of the flow phenomenon started earlier--temporarily interrupted--and finally culminating in shear under a plane strain configuration. Further verification is continuing.

Table VI summarizes some of the reduction of area data for several of the materials and reveals some interesting results. Consider first the conventionally determined R.A. - this turns out to be approximately, for the specific specimen used for this calculation, 62 percent for the copper Cu-II and SAE 1020 steel and 59 percent for the SAE 8620 steel. However, at the onset of cracking, the R.A.'s are only 47, 45, and 43 percent, respectively. In the crack propagation stage or tearing state, the R.A. increases to 57.8, 58.5, and 56.2 percent, respectively; and the last increment in R.A. occurs during the shear separation phase. Percentagewise, the contribution to the ultimate R.A. is predominantly in the region between incipient necking and incipient fracture, though some 24 to 28 percent of the total R.A. occurs after incipient fracture.

28. Effective stresses and strains as used herein are defined in terms of the principal coordinate as follows (where all strains are natural strains):

$$\sigma_{\text{eff}} = \frac{\sqrt{2}}{2} \sqrt{(\sigma_1 - \sigma_2)^2 + (\sigma_1 - \sigma_3)^2 + (\sigma_2 - \sigma_3)^2}$$

$$\epsilon_{\text{eff}} = \frac{\sqrt{2}}{3} \sqrt{(\epsilon_1 - \epsilon_2)^2 + (\epsilon_1 - \epsilon_3)^2 + (\epsilon_2 - \epsilon_3)^2}$$

Note further that though these all have approximately the same total R.A. and, in particular, the same R.A. at incipient fracture, the distribution in the stages prior to incipient fracture is considerably different in the different materials; the copper was able to sustain 76 percent of the ultimate R.A. in the necking process though essentially a zero uniform strain. The SAE 1020 and SAE 8620, on the other hand, exhibited only 46 to 48 percent of the total percent R.A. in the necking process but did absorb 24.4 to 25.8 percent of the total percent R.A. in the prior uniform (non-necking) deformation. In terms of the material strains, again the copper exhibits a nonuniform strain approximately 50 percent in excess of either the SAE 1020 or SAE 8620 with a corresponding loss in the uniform strain.

The point to be emphasized here is that if R.A. is to be a measure of ductility, perhaps one should specify separately both the "uniform" R.A. and the necking R.A. - not at separation but at incipient cracking. It is expected that the R.A. at incipient cracking is indeed a characteristic of the material and is size independent in ductile materials; whereas, the conventionally determined R.A. is size dependent. [29,30,31]

It is interesting to note that the present results indicate that the major part of the deformation occurs in the necking process prior to any significant cracking or void formation. This is in contrast to the conclusions of Gurland and Plateau, [22] who suggest the greatest contribution to deformation to be due to growth of cracks.

CONCLUSIONS

On the basis of the tests of the ductile metals described herein, it is concluded that:

1. Incipient fracture occurs by microscopic void and/or crack formation after neck initiation but before the point normally used for fracture stress determination. The incipient fracture occurs in the region of the neck and is detectable nondestructively by the ultrasonic "search" technique described herein.
2. At loads intermediate to the ultimate and at incipient shear separation, the density of voids and microscopic cracks grows, and the domain occupied with these expands.
3. The stresses at incipient fracture, calculated using the Bridgman analysis, leads to fracture stresses intermediate between the tensile strength and the conventionally determined fracture strength based upon final rapid fracture in a relatively soft machine.

29. DeSisto, T., Carr, F., and Larson, F., U. S. Army Materials Research Agency Report AMRA TR 64-05, February 1964.

30. Williams, T., and Hall, H., Armament Research and Development Est., Fort Holstead, Kent, England, ARDE Report (MX) 1/58, January 1958.

31. Miklowitz, J., Journal of Applied Mechanics, June 1950, pp. 159-168.

4. Gross macroscopic cracks are not evident in the interior of the neck of a tensile specimen until the load-deformation curve has exceeded the final "knee".

5. The final knee in the load-deformation curve is associated with the initiation, growth, and development of the final shear lip, i.e., with incipient shear-separation.

6. The usually observed rapid final fracture of a ductile specimen is a function of the stiffness of the testing machine and specimen; by using a "hard" machine, this rapid separation can be suppressed. The fracture appearance, nevertheless, is relatively unaltered and the shear lip is not suppressed in using a hard machine.

7. The final shear separation, which can be completely controlled, is not, of necessity, an adiabatic process.

8. This final shear separation may very well be a continuation of the earlier flow and necking process under a stress state approaching a plane strain condition.

9. The usually measured R.A. reflects not only the results of a flow process but also the complication associated with void and/or crack propagation and, as such, is size dependent. A modified R.A. measure based upon the configuration at incipient fracture is believed to be a more meaningful measure of ductility.

ACKNOWLEDGMENT

The writers wish to acknowledge (a) Messrs. P. McEleney, R. McIntyre, and C. Berryman for providing the ultrasonic detection "know how"; (b) Messrs. F. Cotter and J. Shippie for their concentrated efforts in the metallographic "searching" task; (c) Mr. M. Menaker for his fine craftsmanship in preparing our RAT and much associated equipment; (d) Messrs. S. Nanfria, J. Reagan, J. Hannon, W. Foster, M. Benicek, and R. Lamothe for preparing the many photographs and drawings; and (e) Mrs. E. O'Toole for preparing the manuscript.

Table I. CHEMICAL ANALYSIS OF MATERIALS INVESTIGATED
(Composition - Percent by Weight)

	Cu	Fe	C	Mn	Si	Ni	Cr	Mo	N	P	S
Copper Cu-I					(NOT DETERMINED)						
SAE 1026 Steel	-	-	0.275	0.93	-	-	-	-	-	0.016	0.027
SAE 4340 Steel	-	-	0.39	0.80	0.32	1.87	0.81	0.28	-	0.010	0.013
Copper Cu-II (URS)	99.94	0.004	-	-	-	-	-	-	-	-	-
SAE 1020 Steel	-	-	0.20	0.46	0.04	0.02	0.05	0.01	0.005	0.015	0.022
SAE 8620 Steel	-	-	0.21	0.99	0.23	0.70	0.51	0.22	-	0.002	0.009

Table II. TENSILE PROPERTIES OF MATERIALS INVESTIGATED AT ROOM TEMPERATURE

Material	Yield Strength*		Tensile Strength† (psi)	Fracture Strength‡ (psi)	Elongation** (%)	Reduction of Area (%)
	0.1% (psi)	0.2% (psi)				
Copper Cu-I (c)	nd	nd	45,200	-	18.0	58.0
SAE 1026 Steel	nd	nd	101,000	-	nd	43.4
SAE 4340 Steel	166,600	166,500	173,500	-	21.9	52.5
Copper Cu-II (URS)	40,400	41,600	42,100	73,000	25.0	60.5
SAE 1020 Steel (GRS)	36,100	36,500	60,400	116,500	39.1	62.0
SAE 8620 Steel (BRS)	47,800	46,900	77,400	141,400	37.5	59.3

*A alloy band extensometer was used under the head to obtain load-elongation curves, therefore yield strengths given are approximate values.

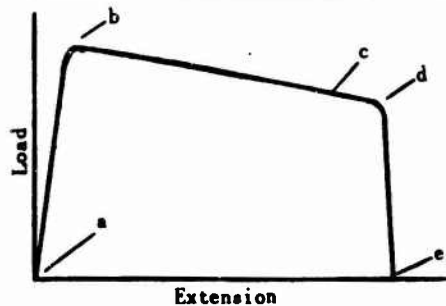
†Conventional, based upon original area.

‡Conventional, based upon the load at incipient shear and the final area.

**Percent Elongation was measured over a 0.64-inch gage length using specimen with 0.252-inch diameter.

Table III. COPPER - UR

			S1	S2	S3	S4	A
^a Initial State	1 Diameter (in)	D_o	←				
^b Incipient Necking	2 Load (lb)	P_n	2095	2065	2065	2080	20
	3 Diameter (in)	D_n	←				
	4 Reduction of Area (%)	RA_n	←				
	5 Tangential Strain (in/in)	$\epsilon_{\theta n} = \ln D_o/D_n$	←				
	6 Radial Strain (in/in)	$\epsilon_{rn} = \epsilon_{\theta n}$	←				
	7 Longitudinal Strain (in/in)	$\epsilon_{sn} = \epsilon_{off} = 2 \ln D_o/D_n$	←				
	8 Longitudinal Stress (ksi) (true)	$\sigma_{sn} = \sigma_{off}$	43.0	42.4	42.4	42.7	4
	^c Incipient Fracture	9 Load (lb)	P_c				
10 Diameter - Minimum in Neck (in)		D_c					
11 Profile Radius of Neck (in)		R_c					
12 Reduction of Area (%)		RA_c					
13 Tangential Strain (in/in)		$\epsilon_{\theta c} = -\ln D_o/D_c$					
14 Radial Strain (in/in)		$\epsilon_{rc} = \epsilon_{\theta c}$					
15 Longitudinal Strain (in/in)		$\epsilon_{sc} = 2 \ln D_o/D_c$					
16 Tangential Stress (ksi) (At Axis of Necked Region)		$\sigma_{\theta c}$					
17 Radial Stress (ksi)		σ_{rc}					
18 Longitudinal Stress (ksi)		σ_{sc}					
19 Effective Strain (in/in)		ϵ_{eff}					
20 Effective Stress (ksi)	σ_{eff}						
^d Incipient Shear	21 Load (lb)	P_s	1460	1450/1425†	1430	1490	1425
	22 Diameter - Minimum in Neck (in)	D_s		.166			
	23 Crack Diameter (in)**	d_s	.064±.003				
	24 Profile Radius of Neck (in)	R_s		.14			
	25 Reduction of Area (%)	RA_s		56.7			5
	26 Tangential Strain (in/in)	$\epsilon_{\theta s} = -\ln D_o/D_s$		-.416			-
	27 Radial Strain (in/in)	$\epsilon_{rs} = \epsilon_{\theta s}$		-.416			-
	28 Longitudinal Strain (in/in)	$\epsilon_{ss} = 2 \ln D_o/D_s$.831			.
	29 Tangential Stress (ksi)	$\sigma_{\theta s} = 1/2 \sigma_{ss}$		38.6			3
	30 Radial Stress (ksi)	$\sigma_{rs} = 0$		0			
	31 Longitudinal Stress (ksi)	$\sigma_{ss} = P_s / [\pi/4 (D_s^2 - d_s^2)]$		77.3			7
	32 Effective Strain (in/in)	ϵ_{eff}		.831			.
	33 Effective Stress (ksi)	σ_{eff}		66.9			6
^a Final State	34 Diameter (in)	D_f	.158				
	35 Reduction of Area (%) (apparent)	RA_f	60.6				
	36 Effective Strain (in/in) (apparent)	$\epsilon_{xf} = 2 \ln D_o/D_f$.931				



*An S prefix implies testing in a standard testing machine.
 †As A prefix implies testing in the Rigid AMRA Tester.

†Incipient shear calculations were based upon this load.

‡Based upon results of other specimens, loading of this specimen.

**Post separation diameters d_s were measured only on specimen S1 (see sketch). For other specimens, the average value was used.

ble III. COPPER - URS SERIES

Specimen Identification*														Avg.
S2	S3	S4	A5	S6	A7	A8	A9	A10	A11	S12	S13	S14		
					0.252 ± 0.001									0.252
2065	2065	2080	2075	2085	2075	2075	2075	2040	2065	2105	2085	2075	2075	2075
						.249								.249
						2.4								2.4
						-.012								-.012
						-.012								-.012
						.024								.024
42.4	42.4	42.7	42.6	42.8	42.6	42.6	42.6	41.9	42.4	43.2	42.8	42.6	42.6	42.6
						1635			1685	1625	1700	1660	1660	1660
						.179			.189	.178	.186	.185	.183	.183
						.23			.28	.23	.25	.25	.25	.25
						49.6			43.8	50.2	45.2	46.1	47.0	47.0
						-.342			-.288	-.346	-.304	-.310	-.317	-.317
						-.342			-.288	-.346	-.304	-.310	-.317	-.317
						.683			.576	.692	.608	.620	.634	.634
						10.35			8.76	10.3	10.0	9.64	9.81	9.81
						10.35			8.76	10.3	10.0	9.64	9.81	9.81
						70.0			64.5	69.5	67.0	66.4	67.5	67.5
						.683			.576	.692	.608	.620	.634	.634
						59.6			55.7	59.2	57.0	56.8	57.7	57.7
1450/1425†	1430	1490	1425/1380†	1350†	1435/1335†	1405	1375/1320†	1440/1360†	1335/1280†	1430	1490†‡	1550†‡	1425	1425
.166			.164	.160	.163		.164	.163	.161		.167	.173	.165	.165
				.064±.003						.065±.003			.064	.064
.14			.14	.14	.14		.14	.14	.13		.16	.17	.145	.145
56.7			57.6	59.4	58.1		57.6	58.1	59.2		56.0	52.9	57.6	57.6
-.416			-.430	-.454	-.435		-.430	-.436	-.448		-.412	-.375	-.426	-.426
-.416			-.430	-.454	-.435		-.430	-.436	-.448		-.412	-.375	-.426	-.426
.831			.859	.908	.870		.860	.871	.896		.824	.751	.852	.852
38.6			38.5	40.0	37.8		36.9	38.5	37.5		39.8	38.3	38.4	38.4
0			0	0	0		0	0	0		0	0	0	0
77.3			77.0	80.0	75.6		73.8	77.0	75.0		79.7	76.6	76.9	76.9
.831			.859	.908	.870		.860	.871	.896		.824	.751	.852	.852
66.9			66.7	69.3	65.5		63.9	66.7	65.0		69.0	66.3	66.6	66.6
				.160						.156			.158	.158
				59.4						61.6			60.5	60.5
				.908						.960			.931	.931

testing in a standard testing machine.
 testing in the Rigid AMRA Tester (RAT).

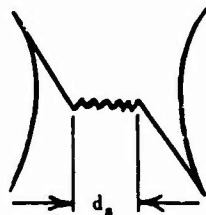
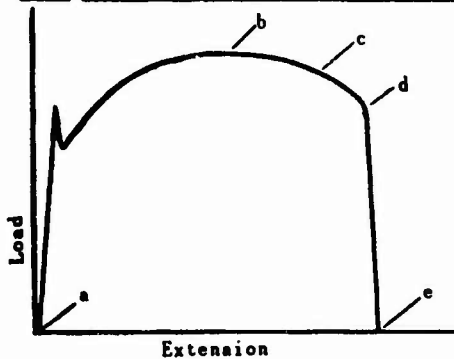
calculations were based upon this load.

of other specimens, loading of this specimen was stopped just prior to the knee.

measurements were measured only on Specimens S1, S6 and S12 and represent the diameters of the flat region of the fracture
 other specimens, the average values were used.

Table IV. SAE 1020 STEEL

			S1	S2	A3	A4	A5	S6
^a Initial State	1 Diameter (in)	D_0	←					
^b Incipient Necking	2 Load (lb)	P_n	2910	2940	2950	2910	2950	2950
	3 Diameter (in)	D_n	←					
	4 Reduction of Area (%)	RA_n	←					
	5 Tangential Strain (in/in)	$\epsilon_{\theta n} = -\ln D_0/D_n$	←					
	6 Radial Strain (in/in)	$\epsilon_{rn} = \epsilon_{\theta n}$	←					
	7 Longitudinal Strain (in/in)	$\epsilon_{zn} = \epsilon_{eff} = 2 \ln D_0/D_n$	←					
	8 Longitudinal Stress (ksi) (true)	$\sigma_{zn} = \sigma_{eff}$	70.1	70.8	71.0	70.1	71.0	71.0
	^c Incipient Fracture	9 Load (lb)	P_c					
10 Diameter - Minimum in Neck (in)		D_c						
11 Profile Radius of Neck (in)		R_c						
12 Reduction of Area (%)		RA_c						
13 Tangential Strain (in/in)		$\epsilon_{\theta c} = -\ln D_0/D_c$						
14 Radial Strain (in/in)		$\epsilon_{rc} = \epsilon_{\theta c}$						
15 Longitudinal Strain (in/in)		$\epsilon_{zc} = 2 \ln D_0/D_c$						
16 Tangential Stress (ksi) (At Axis of Necked Region)		$\sigma_{\theta c}$						
17 Radial Stress (ksi)		σ_{rc}						
18 Longitudinal Stress (ksi)		σ_{zc}						
19 Effective Strain (in/in)		ϵ_{eff}						
20 Effective Stress (ksi)	σ_{eff}							
^d Incipient Shear	21 Load (lb)	P_s	2220	2210	2120/2050†	2030†	2150/1960†	
	22 Diameter - Minimum in Neck (in)	D_s			.162	.159	.162	
	23 Crack Diameter (in)**	d_s		.100±.008				.100±.008
	24 Profile Radius of Neck (in)	R_s			.16	.16	.16	
	25 Reduction of Area (%)	RA_s			58.7	60.1	58.9	
	26 Tangential Strain (in/in)	$\epsilon_{\theta s} = -\ln D_0/D_s$			-.441	-.460	-.443	
	27 Radial Strain (in/in)	$\epsilon_{rs} = \epsilon_{\theta s}$			-.441	-.460	-.443	
	28 Longitudinal Strain (in/in)	$\epsilon_{zs} = 2 \ln D_0/D_s$.882	.920	.887	
	29 Tangential Stress (ksi)	$\sigma_{\theta s} = 1/2 \sigma_{zs}$			80.4	84.6	77.0	
	30 Radial Stress (ksi)	$\sigma_{rs} = 0$			0	0	0	
	31 Longitudinal Stress (ksi)	$\sigma_{zs} = P_s / [\pi/4(D_s^2 - d_s^2)]$			160.8	169.3	154.1	
	32 Effective Strain (in/in)	ϵ_{eff}			.882	.920	.887	
	33 Effective Stress (ksi)	σ_{eff}			139.2	146.6	133.4	
^e Final State	34 Diameter (in)	D_f	.154	.156				.155
	35 Reduction of Area (%) (apparent)	RA_f	62.8	61.8				62.2
	36 Effective Strain (in/in) (apparent)	$\epsilon_{zf} = 2 \ln D_0/D_f$.986	.959				.972



*Au S prefix implies testing in a standard testing machine.
 Au A prefix implies testing in the Rigid AMRA Tester (RAT).

†Incipient shear calculations were based upon this load.

‡Based upon results of other specimens, loading of this specimen was at

*In testing this specimen, there was a delay of one to two months between testing; a slight strain-aging effect may have been thus introduced.

**Post separation diameters d_s were measured only on Specimens S2, S6, & the fracture (see sketch). For other specimens, the average value was

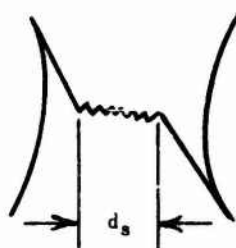
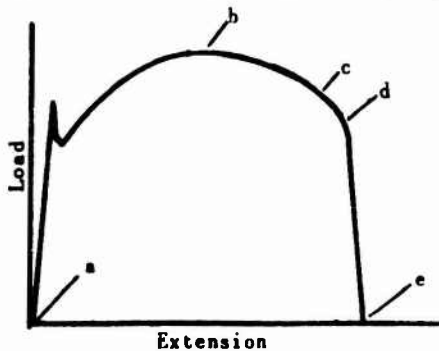
IV. SAE 1020 STEEL - GRS SERIES

Specimen Identification*																Avg.
A4	A5	S6	S7	A8	S9	A10	S11	A12	S13	S14	S15	A16	S17	A18		
					6.252 ± 0.001										0.252	
2910	2950	2950	3010	2930	3020	3000	3040	3000	2950	3000	3010	3000	2950	3050	2976	
					0.230 ± 0.001										0.230	
					16.7										16.7	
					-.091										-.091	
					-.091										-.091	
					.182										.182	
70.1	71.0	71.0	72.5	70.6	72.7	72.2	73.2	72.2	71.0	72.2	72.5	72.2	71.0	73.4	71.6	
				2495		2670	2620	2550	2580	2720		2575		2725	2617	
				.184		.191	.182	.180	.185	.194		.182		.192	.186	
				.32		.58	.40	.33	.42	.72		.31		.56	.46	
				46.8		42.5	47.9	49.0	46.1	40.8		47.8		42.0	45.3	
				-.314		-.277	-.324	-.336	-.307	-.262		-.324		-.271	-.302	
				-.314		-.277	-.324	-.336	-.307	-.262		-.324		-.271	-.302	
				.628		.554	.648	.672	.615	.524		.648		.542	.604	
				11.6		7.08	11.8	11.8	9.55	9.52		12.7		7.35	10.2	
				11.6		7.08	11.8	11.8	9.55	9.52		12.7		7.35	10.2	
				99.4		99.0	108.6	105.5	101.0	95.0		106.2		97.6	101.5	
				.628		.554	.648	.672	.615	.524		.648		.542	.604	
				87.7		91.9	96.8	93.7	91.3	85.5		93.5		90.2	91.3	
50†	2030†	2150/1960†		2200	2250/2100†	2200	2380†+	2360†+	2300††+	2380††+	2240/2150†	2250†	2205††	2275/2160†	2197/2141	
	.159	.162			.162				.164	.167	.163		.162	.163	.163	
			.100±.006		.098±.007		.102±.005								.100	
	.16	.16			.15				.16	.17	.14		.15	.15	.16	
	60.1	58.9			58.9				57.4	56.0	58.2		58.5	58.2	58.3	
	-.460	-.443			-.443				-.429	-.412	-.436		-.443	-.436	-.438	
	-.460	-.443			-.443				-.429	-.412	-.436		-.443	-.436	-.438	
	.920	.887			.887				.838	.825	.872		.787	.872	.876	
	84.6	77.0			80.4				86.7	84.8	82.6		86.4	83.0	82.9	
	0	0			0				0	0	0		0	0	0	
	169.3	154.1			160.8				172.4	169.6	165.3		172.9	166.1	165.9	
	.920	.887			.887				.858	.825	.872		.887	.872	.876	
	146.6	133.4			139.2				150.2	146.8	143.1		149.7	144.1	143.7	
			.155	.156	.155		.154								.155	
			62.2	61.8	62.2		62.8								62.2	
			.972	.960	.972		.986								.973	

Standard testing machine.
 and AMRA Tester (RAT).
 and upon this load.
 loading of this specimen was stopped just prior to the head.
 delay of one to two months between the observation of the first ultrasonic pip and subsequent
 may have been thus introduced.
 measured only on Specimens S2, S6, S9 and S11 and represent the diameters of the flat region of
 specimens, the average value was used.

Table V. SAE 8620 STEEL - BRS

			S1	S2	A3	A4	A5
*Initial State	1 Diameter (in)	D_o					.252
^b Incipient Necking	2 Load (lb)	P_n	3870	3880	3860	3900	3840
	3 Diameter (in)	D_n					.231
	4 Reduction of Area (%)	RA_n					15.9
	5 Tangential Strain (in/in)	$\epsilon_{\theta n} = -\ln D_o/D_n$					-.087
	6 Radial Strain (in/in)	$\epsilon_{rn} = \epsilon_{\theta n}$					-.087
	7 Longitudinal Strain (in/in)	$\epsilon_{zn} = \epsilon_{eff} = 2\ln D_o/D_n$.174
	8 Longitudinal Stress (ksi) (true)	$\sigma_{zn} = \sigma_{eff}$					91.7
	^c Incipient Fracture	9 Load (lb)	P_c				
10 Diameter - Minimum in Neck (in)		D_c					
11 Profile Radius of Neck (in)		R_c					
12 Reduction of Area (%)		RA_c					
13 Tangential Strain (in/in)		$\epsilon_{\theta c} = -\ln D_o/D_c$					
14 Radial Strain (in/in)		$\epsilon_{rc} = \epsilon_{\theta c}$					
15 Longitudinal Strain (in/in)		$\epsilon_{zc} = 2\ln D_o/D_c$					
16 Tangential Stress (ksi) (At Axis of Necked Region)		$\sigma_{\theta c}$					
17 Radial Stress (ksi)		σ_{rc}					
18 Longitudinal Stress (ksi)		σ_{zc}					
19 Effective Strain (in/in)		ϵ_{eff}					
20 Effective Stress (ksi)		σ_{eff}					
^d Incipient Shear	21 Load (lb)	P_s	2900†	3000†	2670	2730	2500†
	22 Diameter - Minimum in Neck (in)	D_s	.157	.161			.161
	23 Crack Diameter (in)**	d_s		.092±.007		.087±.007	.092±.005
	24 Profile Radius of Neck (in)	R_s	.125	.11			
	25 Reduction of Area (%)	RA_s	61.3	59.2			59.1
	26 Tangential Strain (in/in)	$\epsilon_{\theta s} = -\ln D_o/D_s$	-.474	-.448			-.448
	27 Radial Strain (in/in)	$\epsilon_{rs} = \epsilon_{\theta s}$	-.474	-.448			-.448
	28 Longitudinal Strain (in/in)	$\epsilon_{zs} = 2\ln D_o/D_s$.948	.896			.896
	29 Tangential Stress (ksi)	$\sigma_{\theta s} = 1/2 \sigma_{zs}$	111.9	109.4			105.8
	30 Radial Stress (ksi)	$\sigma_{rs} = 0$	0	0			0
	31 Longitudinal Stress (ksi)	$\sigma_{zs} = P_s / [\pi/4(D_s^2 - d_s^2)]$	223.9	218.9			211.6
	32 Effective Strain (in/in)	ϵ_{eff}	.948	.896			.896
	33 Effective Stress (ksi)	σ_{eff}	193.8	189.5			187.2
*Final State	34 Diameter (in)	D_f	.157	.161	.160	.162	.161
	35 Reduction of Area (%) (apparent)	RA_f	61.3	59.2	59.7	58.8	59.1
	36 Effective Strain (in/in) (apparent)	$\epsilon_{zf} = 2\ln D_o/D_f$.948	.896	.908	.883	.896



*An S prefix implies testing in a standard testing machine.

An A prefix implies testing in the Rigid AMRA Tester (RAT)

†Incipient shear calculations were based upon this load.

‡Based upon results of other specimens, loading of this spe

**Post separation diameters d_s were measured only on Specime the fracture (see sketch). For other specimens, the svers

SAE 8620 STEEL - BRS SERIES

Specimen Identification*														Avg.	
2	A3	A4	A5	S6	S9	A10	S11	A12	S13	S14	S15	A16	S17		A18
			.252	.251			.252	.252	.252	.252	.252	.252	.252	.252	.252
80	3860	3900	3840 .231 15.9 -.087 -.087 .174 91.7	3850 .229 16.8 -.091 -.091 .182 93.4	3900	3910	3830 .228 18.1 -.100 -.100 .199 94.0	3850 .228 18.1 -.100 -.100 .199 94.5	3890	4000 .230 16.7 -.091 -.091 .182 96.4	3920 .230 16.7 -.091 -.091 .182 94.4	3915 .230 16.7 -.091 -.096 .182 94.3	3880 .229 17.3 -.096 -.096 .191 94.2	3900 .230 16.7 -.091 -.096 .182 94.0	3887 .229 16.9 -.093 -.093 .186 94.1
							3310 .181 .29 48.3 -.331 -.331 .662 17.45 17.45 140.0 .662 122.5	3500 .1925 .48 41.9 -.268 -.268 .536 10.9 10.9 125.5 .536 114.6	3470 .190 .38 43.1 -.282 -.282 .564 13.65 13.65 131.5 .564 117.8	3500 .186 .46 45.5 -.305 -.305 .610 11.8 11.8 134.2 .610 122.0	3480 .1925 .43 42.0 -.271 -.271 .542 12.08 12.08 127.5 .623 115.4	3550 .196 .30 39.5 -.250 -.250 .500 16.45 16.45 125.8 .500 109.4	3430 .188 .45 44.3 -.291 -.291 .582 11.67 11.67 130.0 .582 118.4	3490 .1915 .50 42.2 -.274 -.274 .548 10.56 10.56 126.0 .548 115.5	3466 .190 .411 43.3 -.284 -.284 .568 13.07 13.07 130.0 .568 116.9
00†	2670	2730	2900†	2920†	2830/2800†	2865/2780†	3040††	3040††	3050		3080††		2880		2888/2940
161			.161	.163	.167	.165	.1675	.1675			.171				.164
±.007		.087±.007	.092±.005	.090±.009											.090
.11				.17	.17	.20	.20	.20			.20				.167
9.2			59.1	58.1	56.1	57.2	55.8	55.8			54.0				57.4
48			-.448	-.431	-.412	-.423	-.408	-.408			-.388				-.426
448			-.448	-.431	-.412	-.423	-.408	-.408			-.388				-.426
896			.896	.862	.824	.846	.815	.815			.775				.853
9.4			105.8	100.5	90.2	92.6	97.0	97.0			92.8				99.7
0			0	0	0	0	0	0			0				0
9.9			211.6	201.1	180.4	185.3	194.1	194.1			185.6				199.4
896			.896	.862	.824	.846	.815	.815			.775				.853
9.5			187.2	158.9	156.2	160.4	168.1	168.1			160.7				171.4
161	.160	.162	.161	.163											.160
9.2	59.7	58.8	59.1	58.1											59.3
896	.908	.883	.896	.862											.900

Testing in a standard testing machine.

Testing in the Rigid AMRA Teeter (RAT).

Measurements were based upon this load.

For other specimens, loading of this specimen was stopped just prior to the knee.

Where d_f were measured only on Specimens S2, A4, A5 and S6 and represent the diameters of the flat region of each. For other specimens, the average value was used.

Table VI. STRAIN DATA

	Copper [60.5% RA]				SAE 1920 [62% RA]				SAE 8620 [59.3% RA]			
	% RA	% (% RA)	$\Delta\%$ (% RA)	ϵ_z	% RA	% (% RA)	$\Delta\%$ (% RA)	ϵ_z	% RA	% (% RA)	$\Delta\%$ (% RA)	ϵ_z
Init. State	0.0	0.0	4.0	0.0	0.0	0.0	26.9	0.0	0.0	0.0	28.5	0.0
Incip. Neck	2.4	4.0		0.02	16.7	26.9		0.18	16.9	28.5		0.19
Incip. Frac.	47.0	77.7	75.7	0.63	45.3	73.1	46.2	0.60	43.3	73.0	44.5	0.57
Incip. Shear	57.6	95.2	17.5	0.86	58.3	94.0	20.9	0.88	57.4	96.8	29.8	0.85
Final	60.5	100.0	4.8	0.93	62.0	100.0	6.0	0.97	59.3	100.0	3.2	0.91

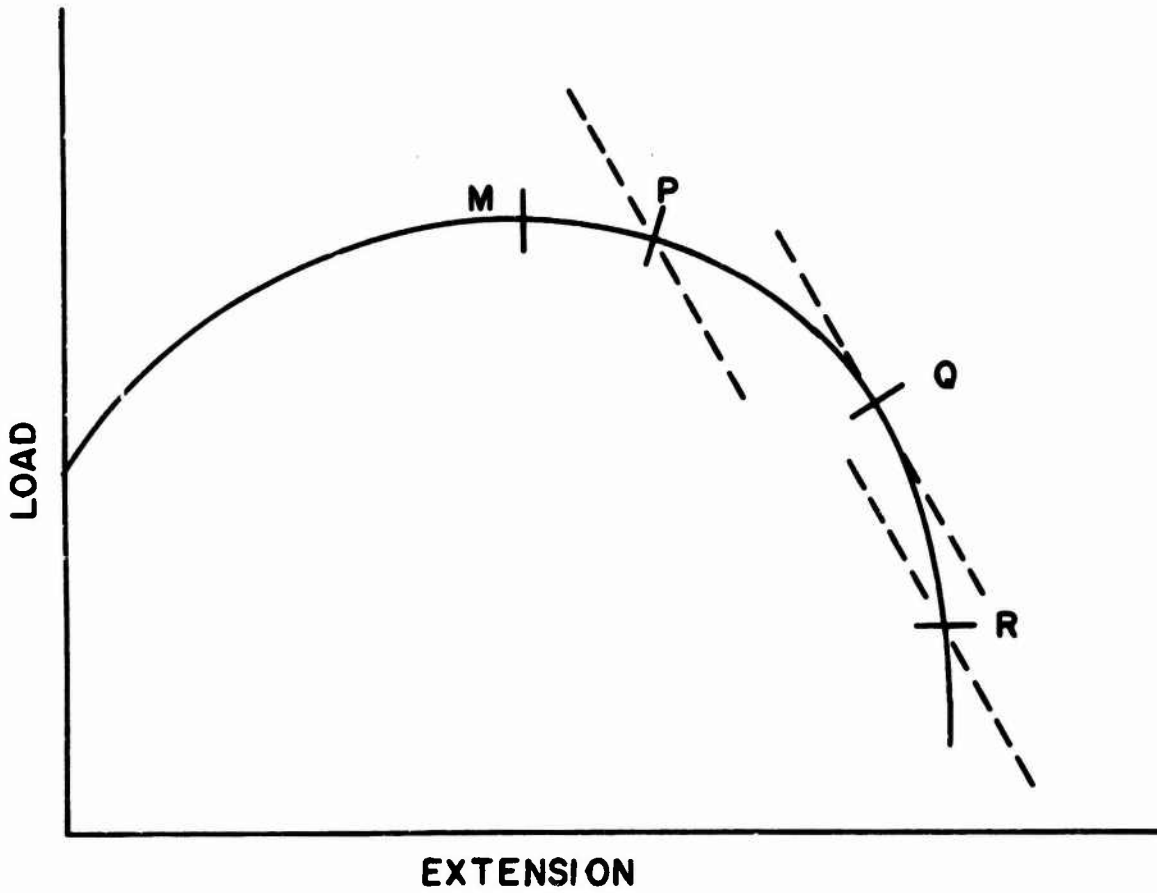
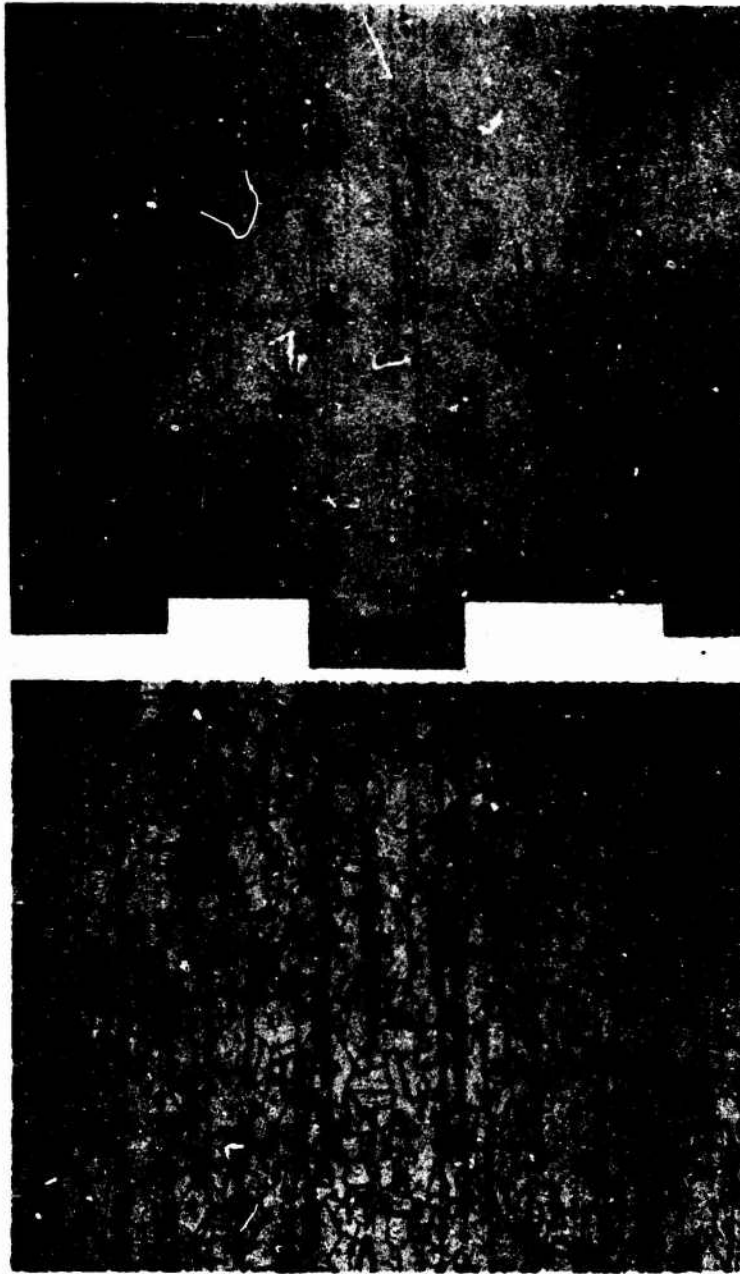


**Fig. 1. CRITERION FOR HIGH VELOCITY DUCTILE FRACTURE
(AFTER OROWAN¹¹)**

U. S. ARMY MATERIALS RESEARCH AGENCY

19-066-706/AMC-65

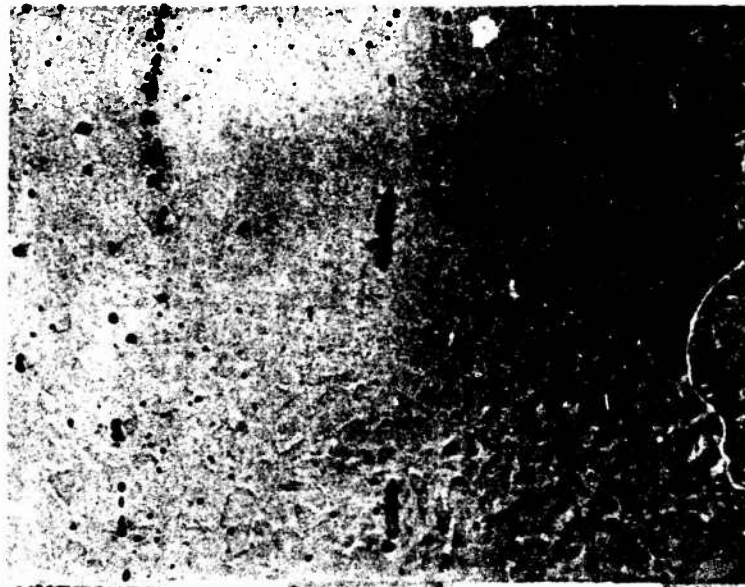


ETCHED COPPER CU II 100X

FIG.2 MICRO STRUCTURE VIRGIN STATE

U. S. ARMY MATERIALS RESEARCH AGENCY

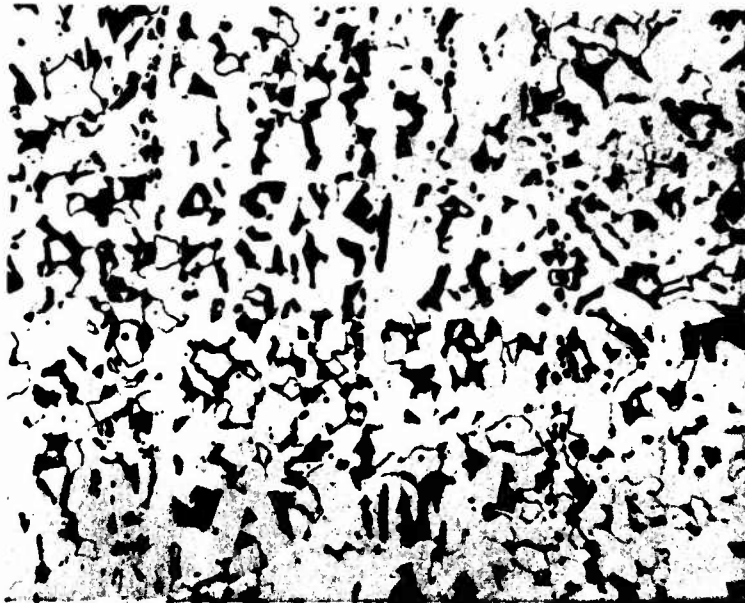
19-066-730/AMC-65



UNETCHED



100X



ETCHED

SAE 1020

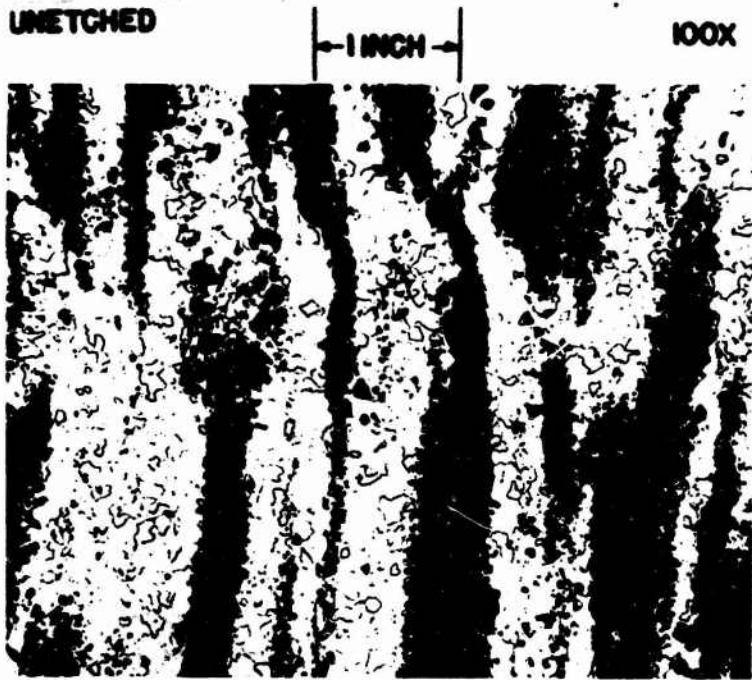
100X

VIRGIN STATE

FIG. 3 MICRO STRUCTURE

U. S. ARMY MATERIALS RESEARCH AGENCY

19-066-714/AMC-65



ETCHED SAE 8620 100X

FIG. 4 MICRO STRUCTURE VIRGIN STATE

U. S. ARMY MATERIALS RESEARCH AGENCY

19-066-715/AMC-65

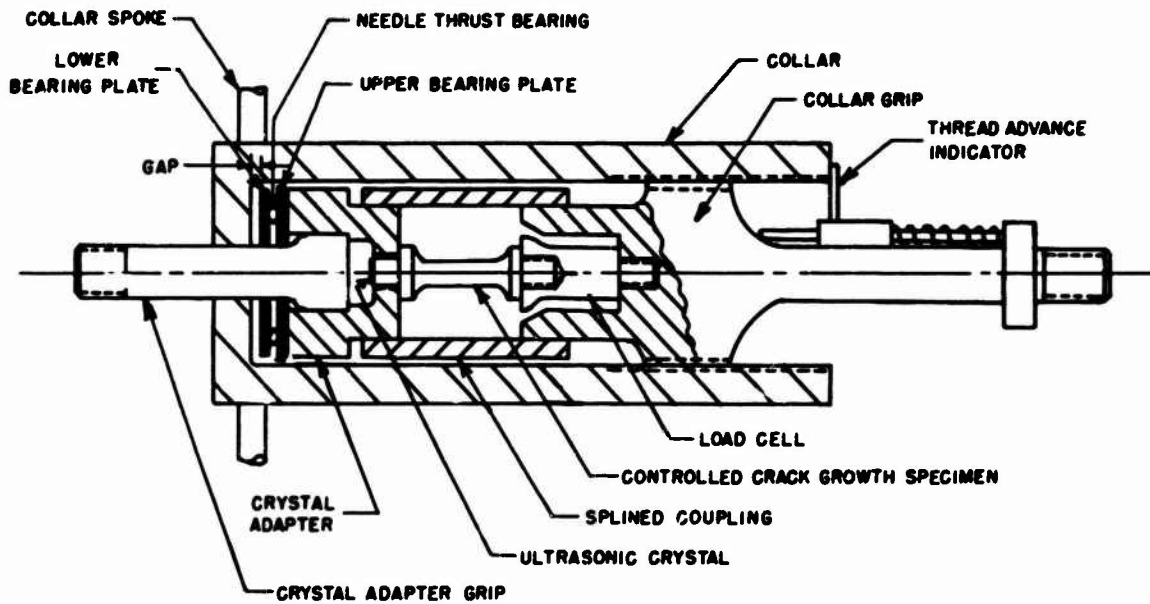


Fig. 5. SCHEMATIC OF RIGID AMRA TESTER (RAT)

U. S. ARMY MATERIALS RESEARCH AGENCY

19-066-704/AMC-65

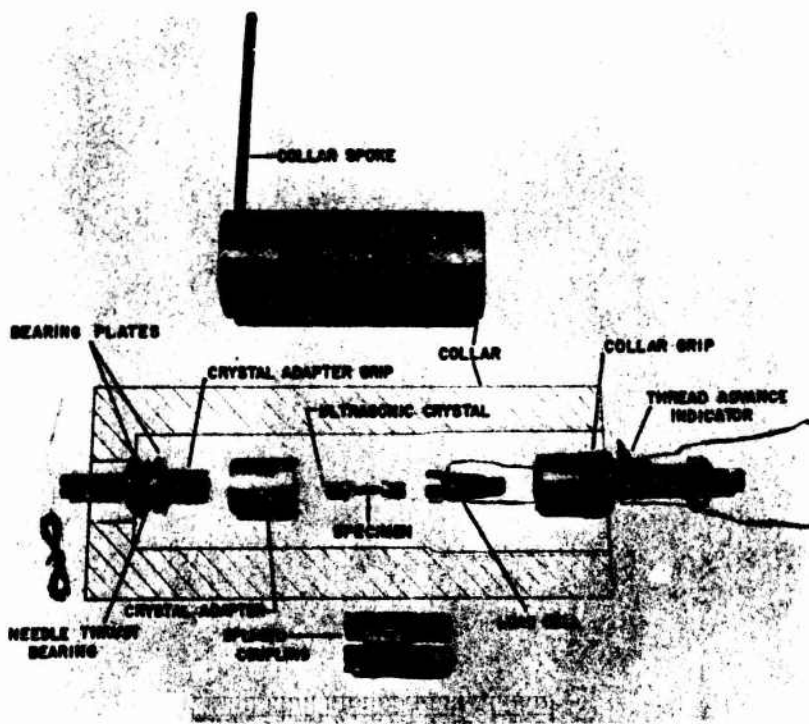


Fig. 6. EXPLODED VIEW OF RIGID AMRA TESTER (RAT)

U. S. Army Materials Research Agency

19-066-514/AMC-66

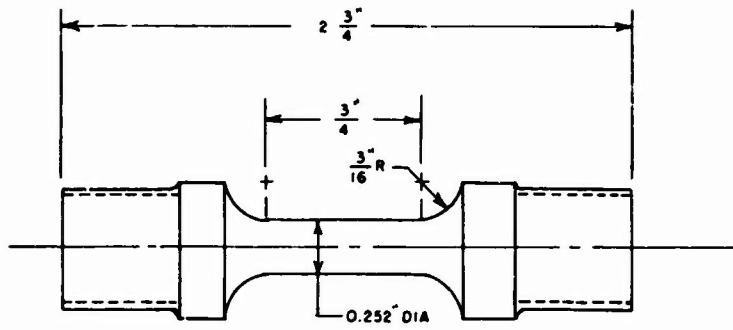


Fig. 7. TENSION SPECIMEN DETAIL
U. S. ARMY MATERIALS RESEARCH AGENCY

19-066-698/AMC-65

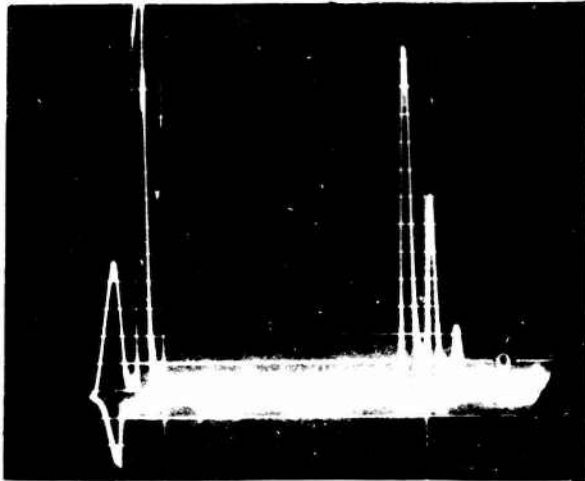


Fig. A
Load = 0

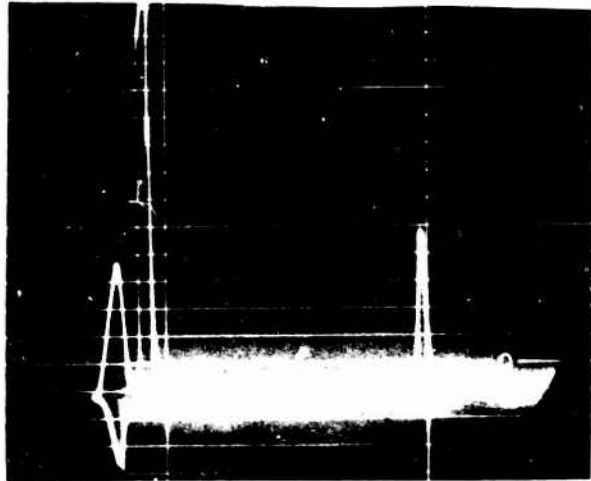


Fig. B
Load = 1760 lb
At the First Ultrasonic Indication (Pip) of
Internal Crack Initiation

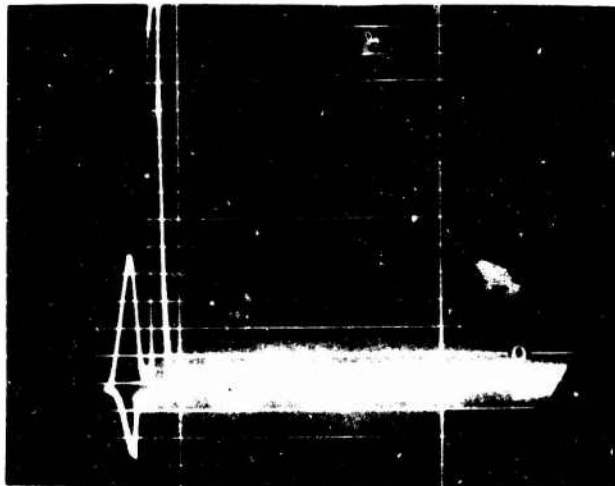


Fig. C
Load = 700 lb
Near the Final Stage
of Complete Fracture

Fig. 8. TYPICAL ULTRASONIC RESPONSE IN COPPER CU I

U. S. ARMY MATERIALS RESEARCH AGENCY

19-066-698/AMC-65

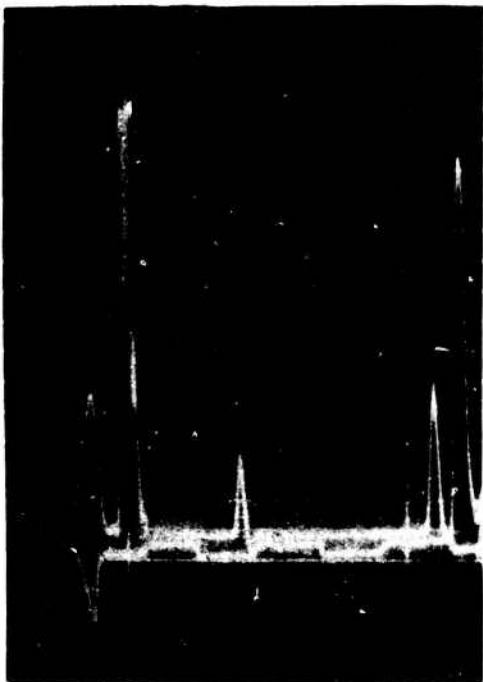


Fig. A
Load = 0

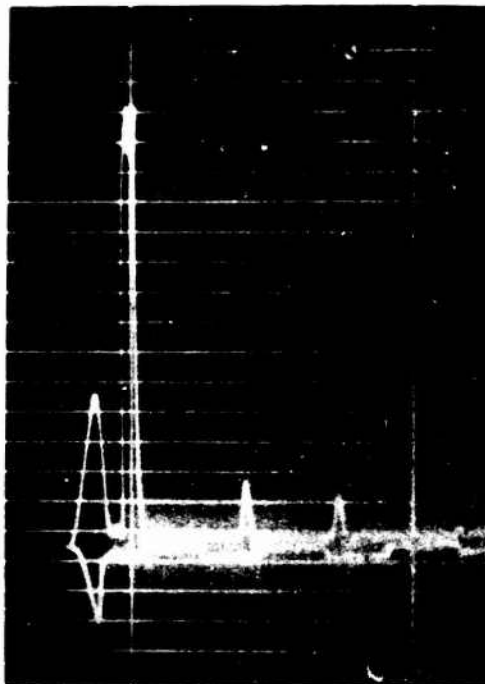


Fig. B
Load Unknown
Taken Soon After the First Ultrasonic
Indication (Pip) of Internal Crack
Initiation

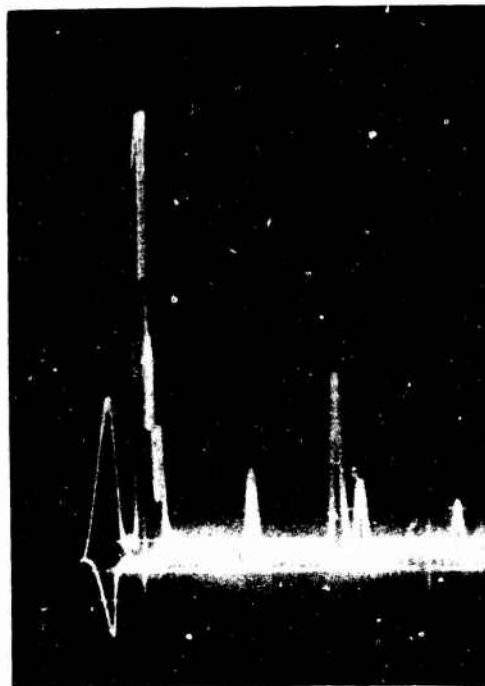


Fig. C
Load Unknown
Near the Final Stage of
Complete Fracture

Fig. 9. TYPICAL ULTRASONIC RESPONSE IN SAE 4340

U. S. Army Materials Research Agency

19-066-697/AMC-64

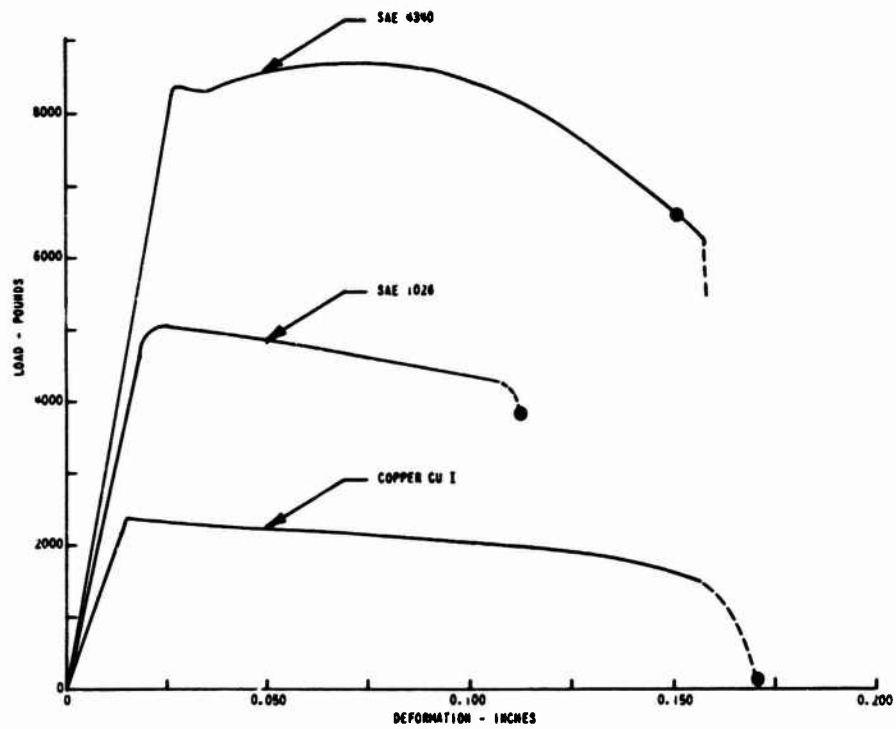
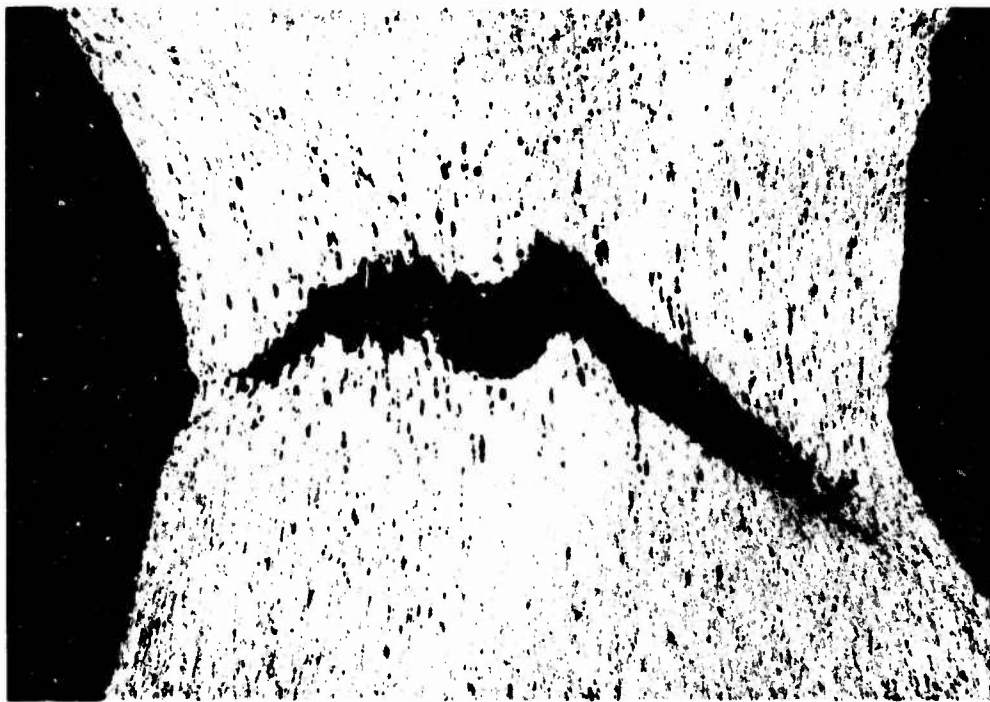


Fig. 10. TYPICAL LOAD DEFORMATION CURVES

U. S. ARMY MATERIALS RESEARCH AGENCY

19-066-705/AM-65



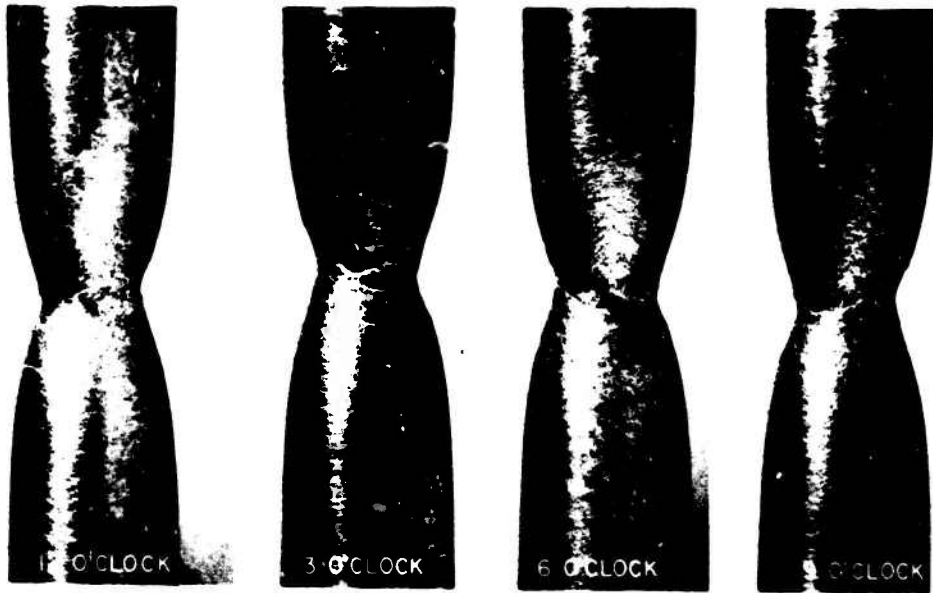
Spec. No. C-2

32X

Fig. 11. MICROSTRUCTURE - COPPER CU I (UNETCHED)

U. S. Army Materials Research Agency

19-066-692/AMC-65



19-066-951/AMC-65

Fig. 12. EXTERIOR VIEWS OF NECKED REGION - COPPER Cu I

U. S. Army Materials Research Agency

19-066-951/AMC-65

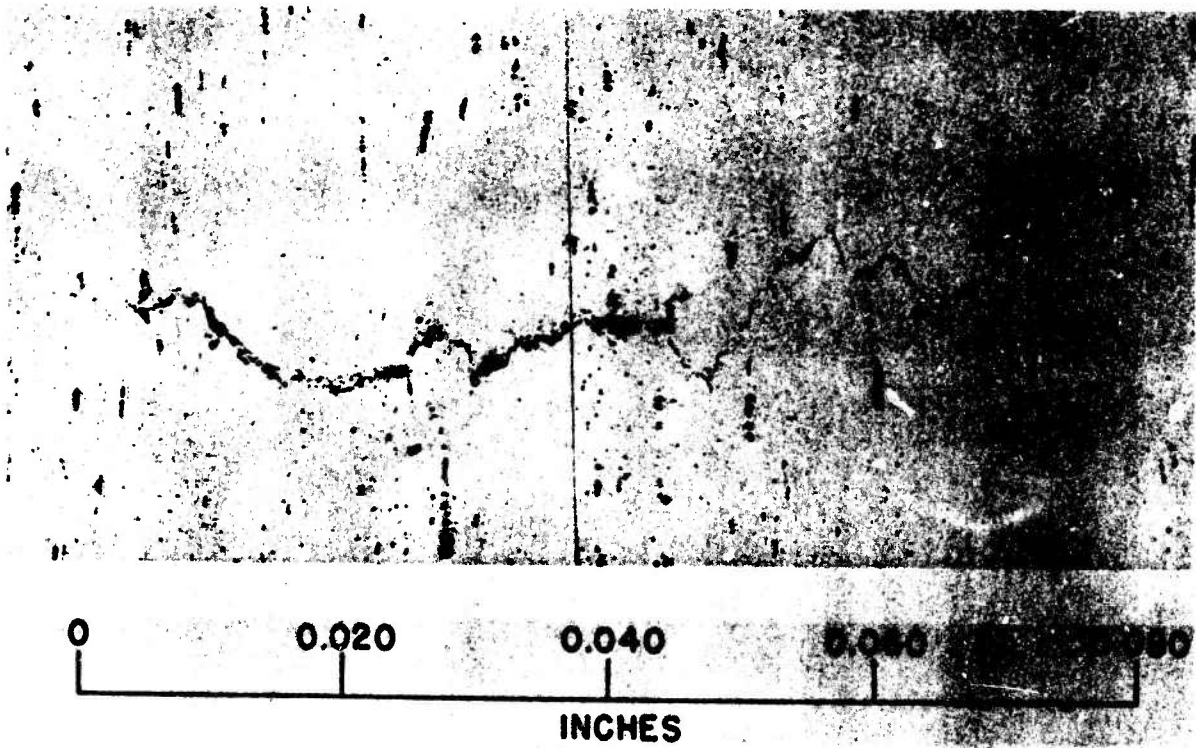


Fig. 13. MICROSTRUCTURE - SAE 1026 (SWTCHED)

U. S. Army Materials Research Agency

19-066-621/AMC-65

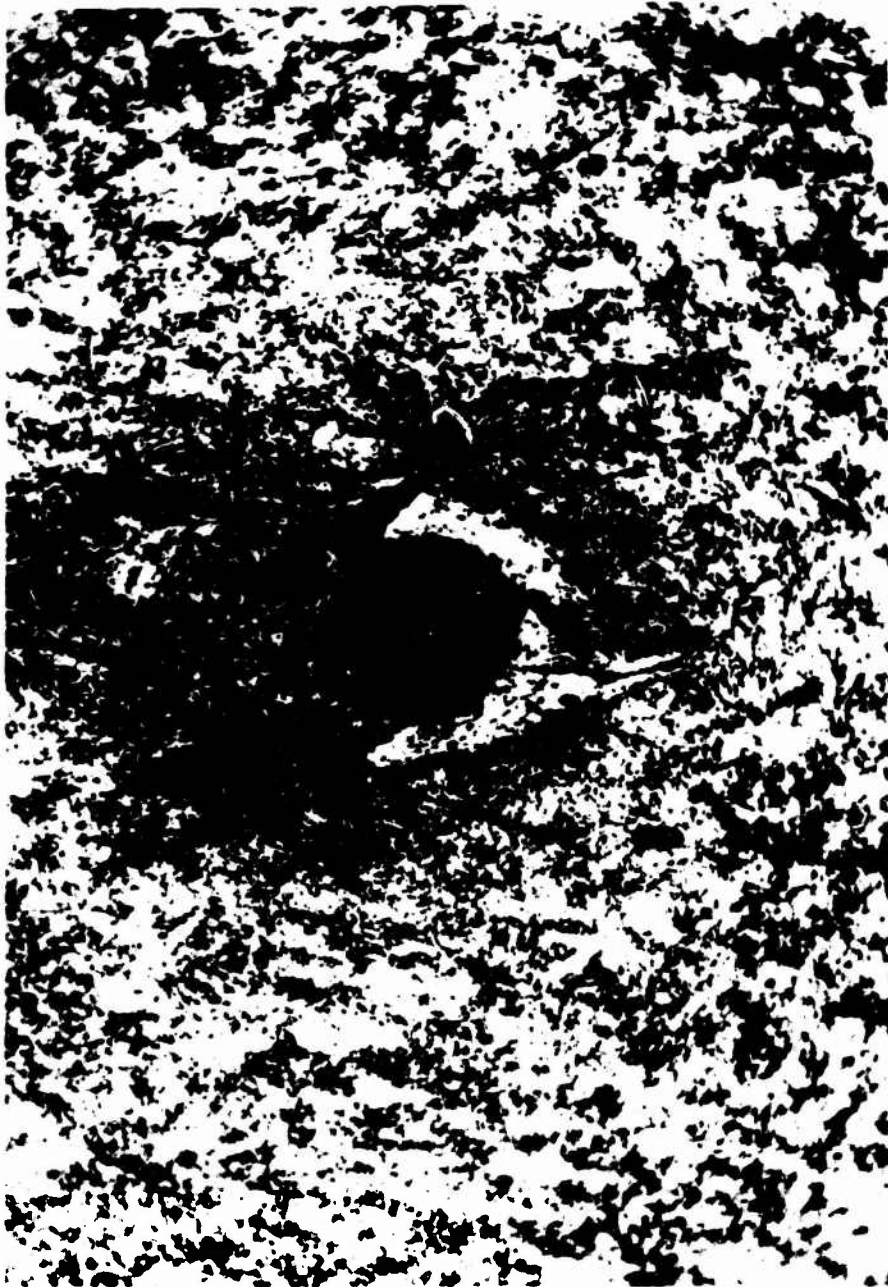


Fig. 14. MICROSTRUCTURE - SAE 4340 (UNETCHED)

1000X

U. S. Army Materials Research Agency

19-066-694/AMC-65

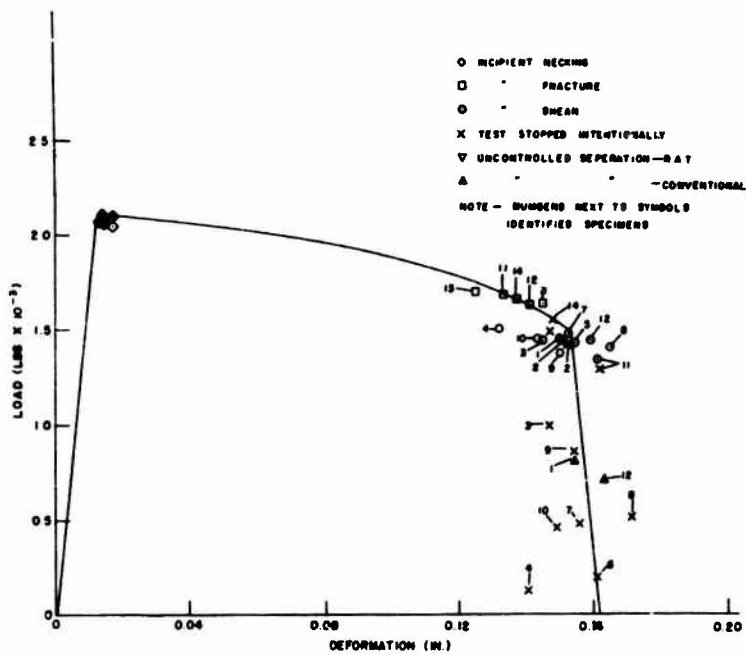


FIG. 15 COMPOSITE LOAD-DEFORMATION CURVE COPPER CU II

U. S. ARMY MATERIALS RESEARCH AGENCY
19-046-735/AMC-65

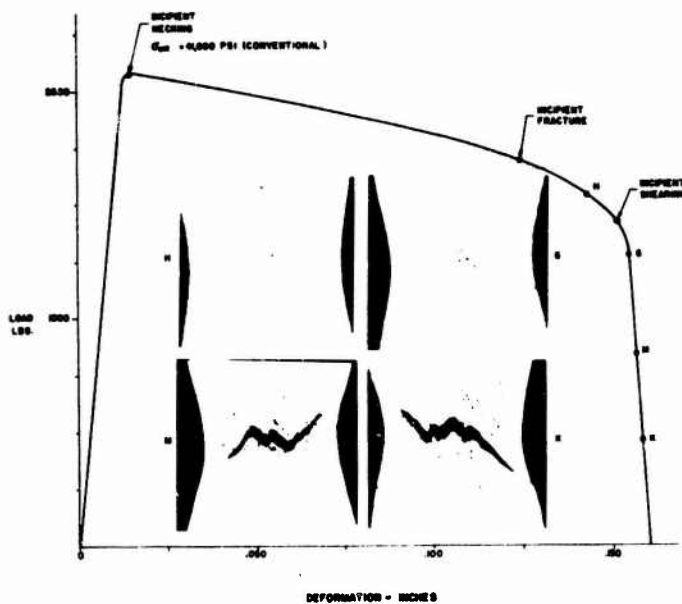


FIG. 16 CORRELATION OF FAILURE PROCESS WITH LOAD DEFORMATION CURVE (Cu II)

U. S. ARMY MATERIALS RESEARCH AGENCY
19-046-730/AMC-65

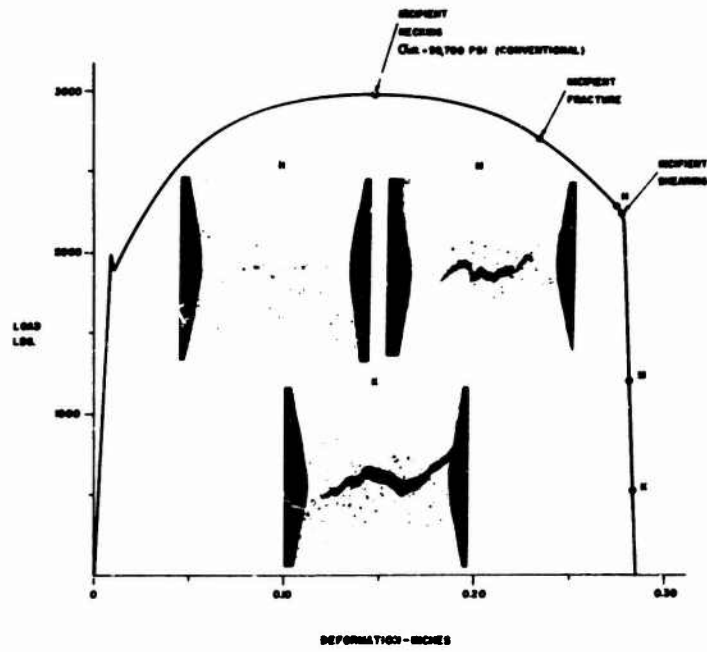


FIG 19 CORRELATION OF FAILURE PROCESS WITH LOAD DEFORMATION CURVE
(STEEL SAE 1020)

U. S. ARMY MATERIALS RESEARCH AGENCY
19-066-739/AMC-65

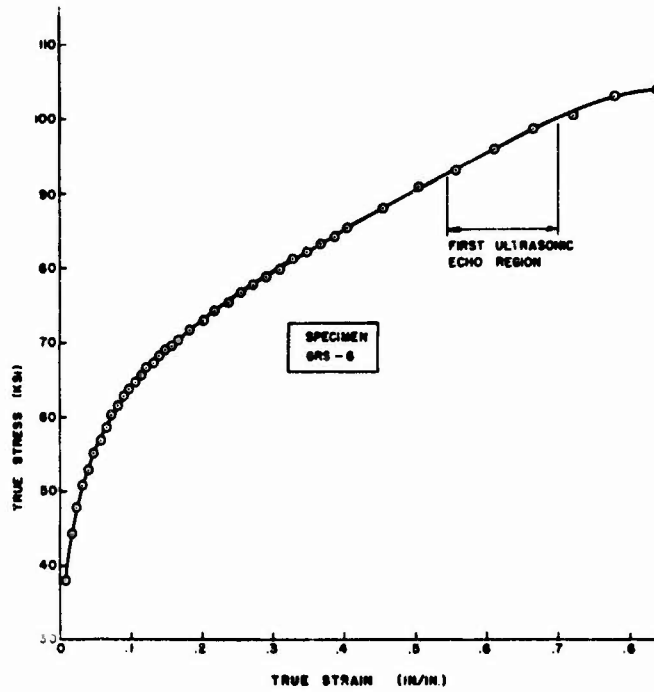


FIG. 20 TRUE STRESS-TRUE STRAIN CURVE SAE 1020

U. S. ARMY MATERIALS RESEARCH AGENCY
19-066-718/AMC-65

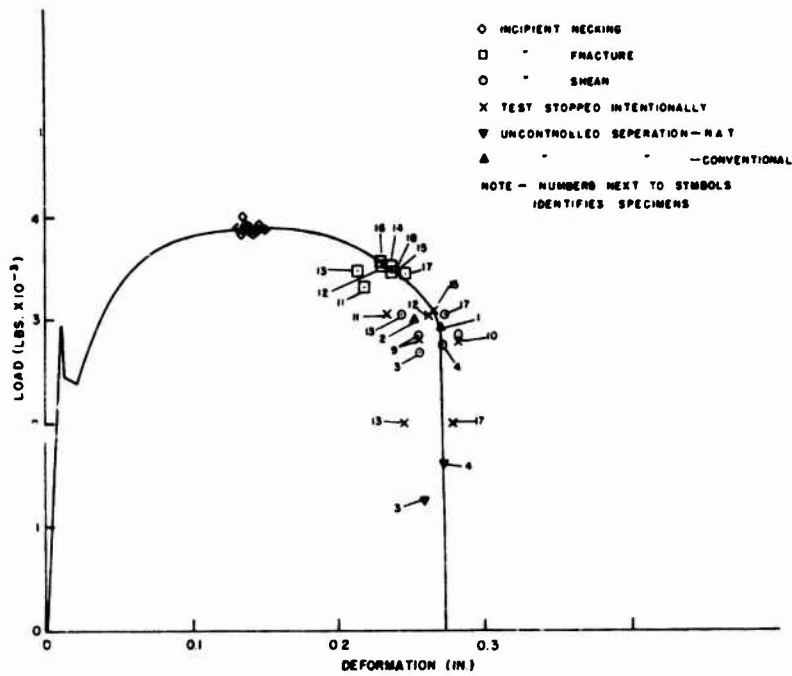


FIG. 21 COMPOSITE LOAD-DEFORMATION CURVE SAE 8620

U. S. ARMY MATERIALS RESEARCH AGENCY
 19-066-736/AMC-65

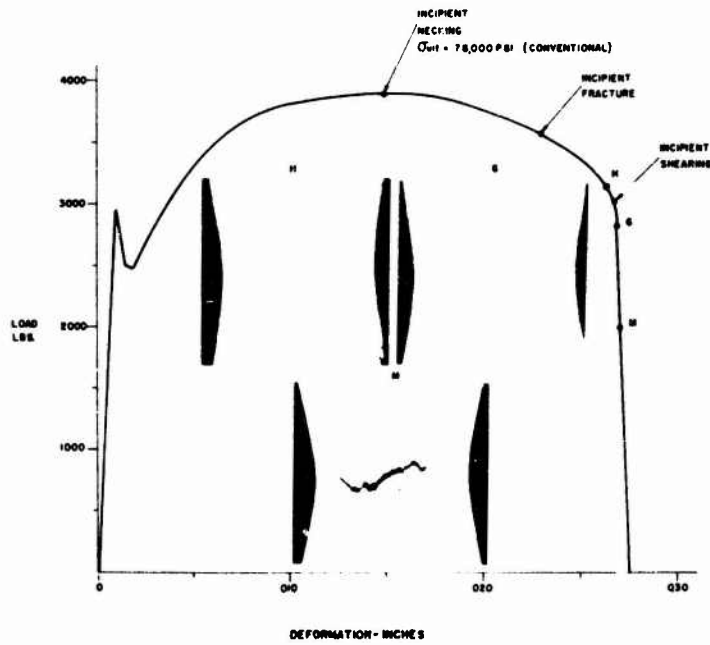


FIG. 22 CORRELATION OF FAILURE PROCESS WITH LOAD DEFORMATION CURVE (STEEL SAE 8620)

U. S. ARMY MATERIALS RESEARCH AGENCY
 19-066-780/AMC-65

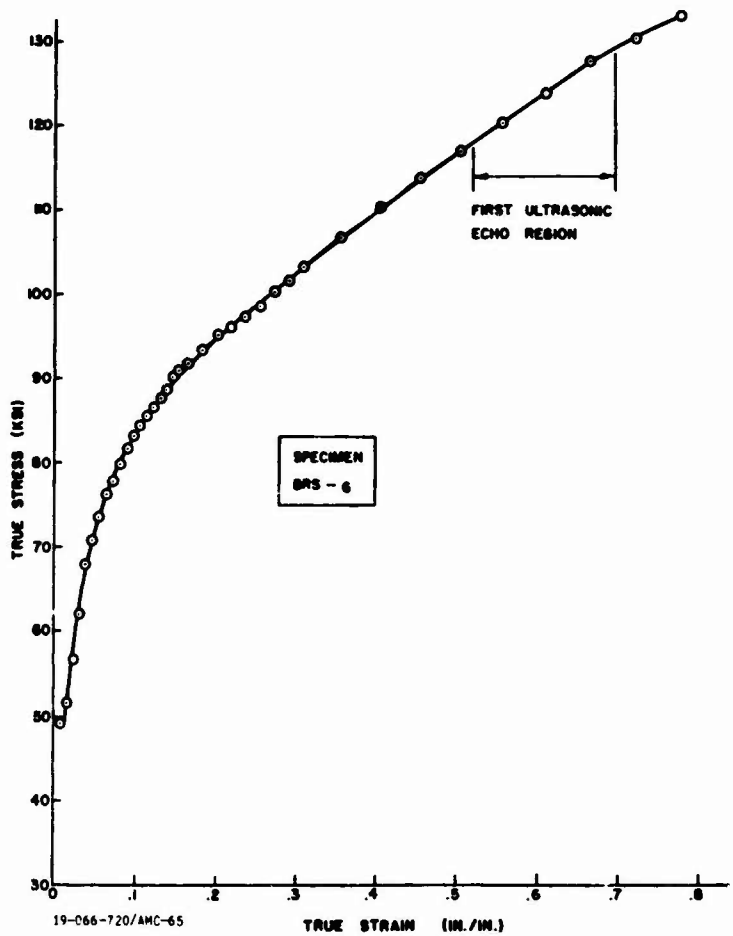


FIG. 23 TRUE STRESS-TRUE STRAIN CURVE SAE 8620

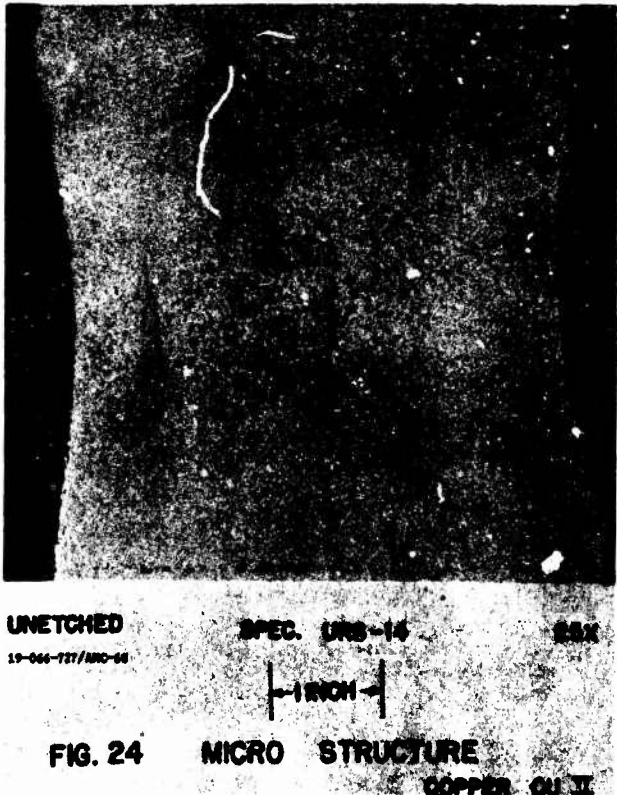


FIG. 24 MICRO STRUCTURE COPPER CU II

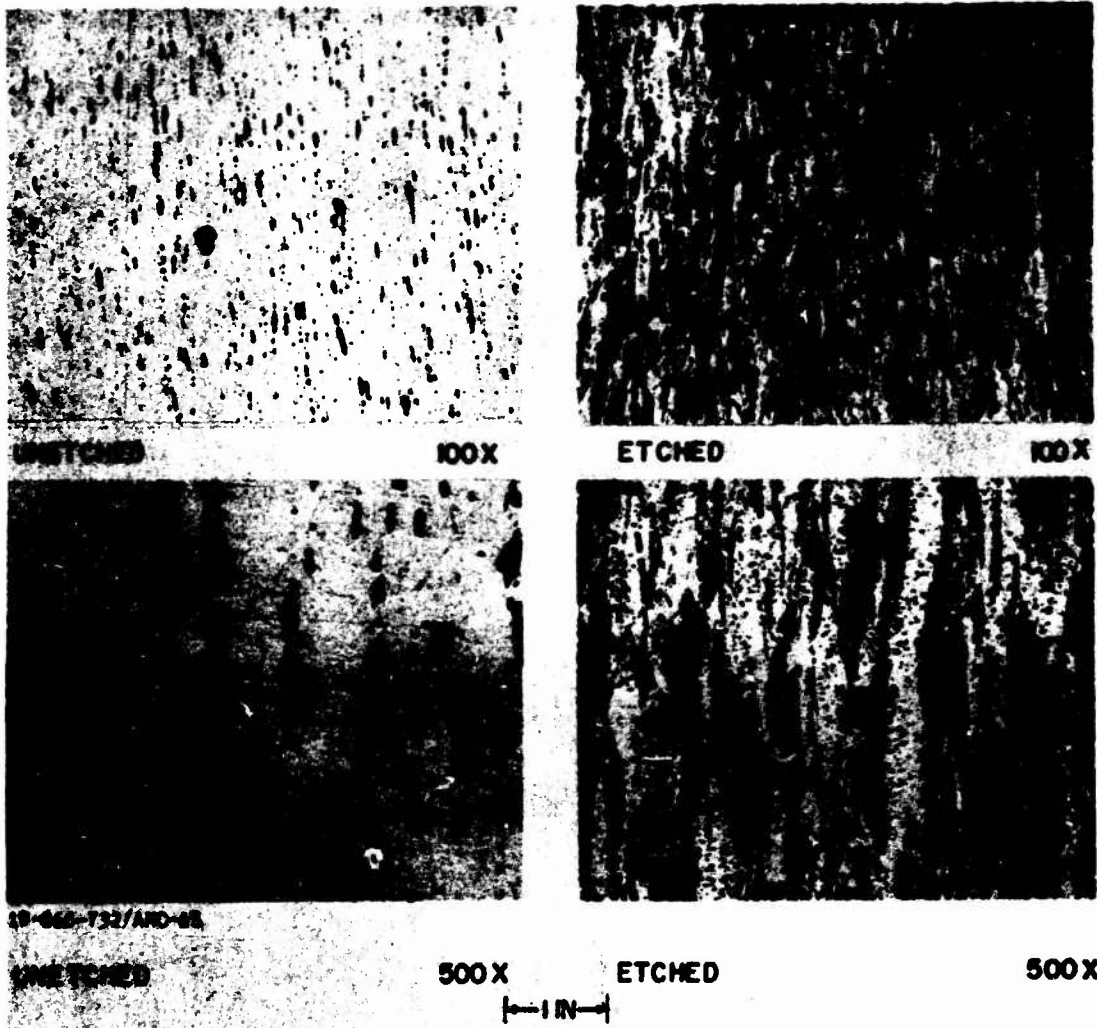


FIG. 25 MICRO STRUCTURE COPPER II SPEC. URS-14

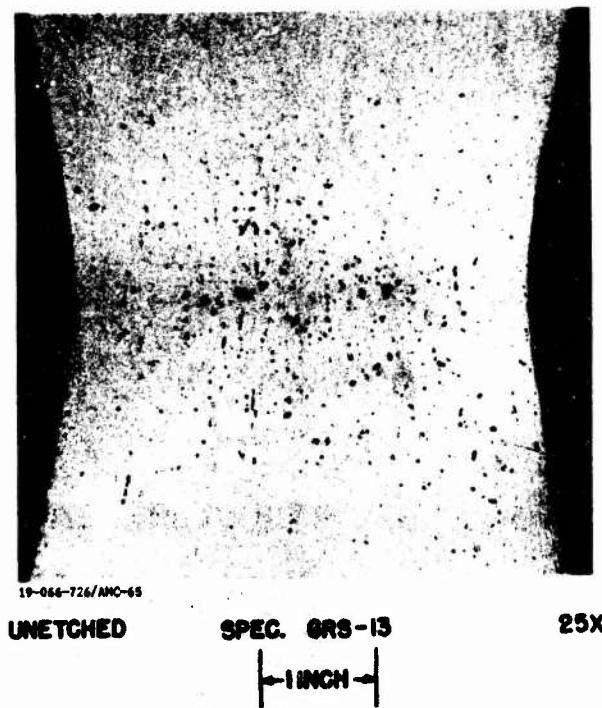


FIG. 26 MICRO STRUCTURE SAE 1020



UNETCHED

100X



UNETCHED

SPEC. GRS-13

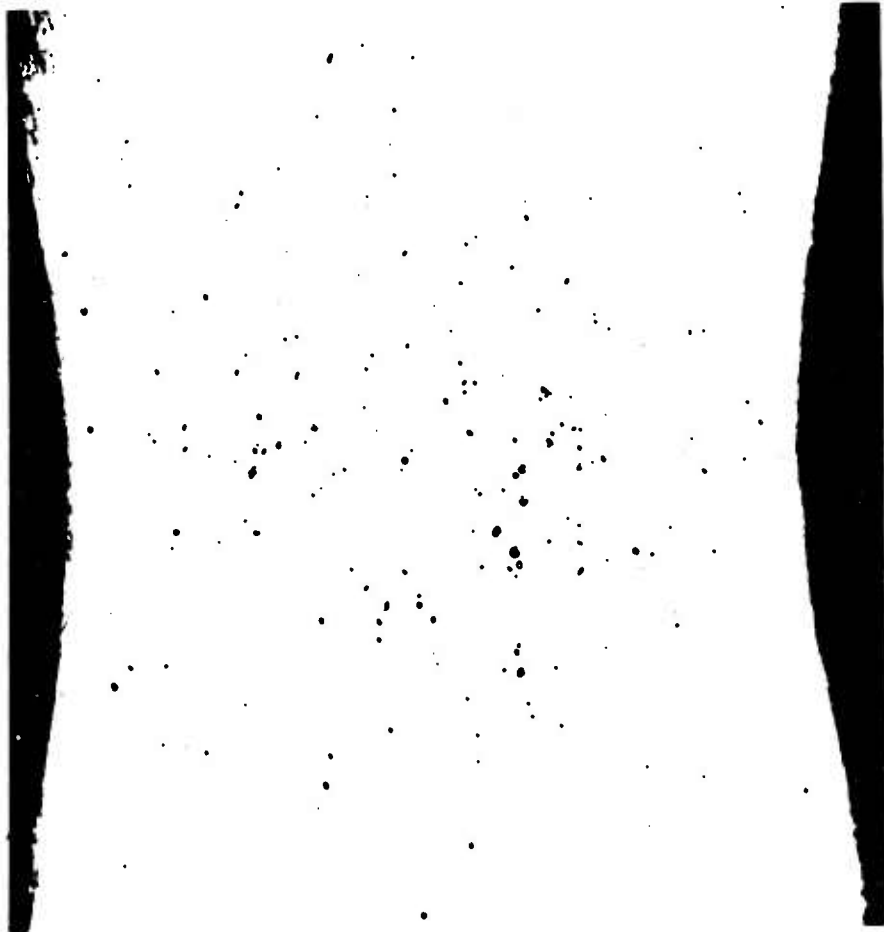
500X



FIG. 27 MICRO STRUCTURE SAE 1020

U. S. ARMY MATERIALS RESEARCH AGENCY

19-066-744/AMC-65



UNETCHED

SPEC. BRS-12

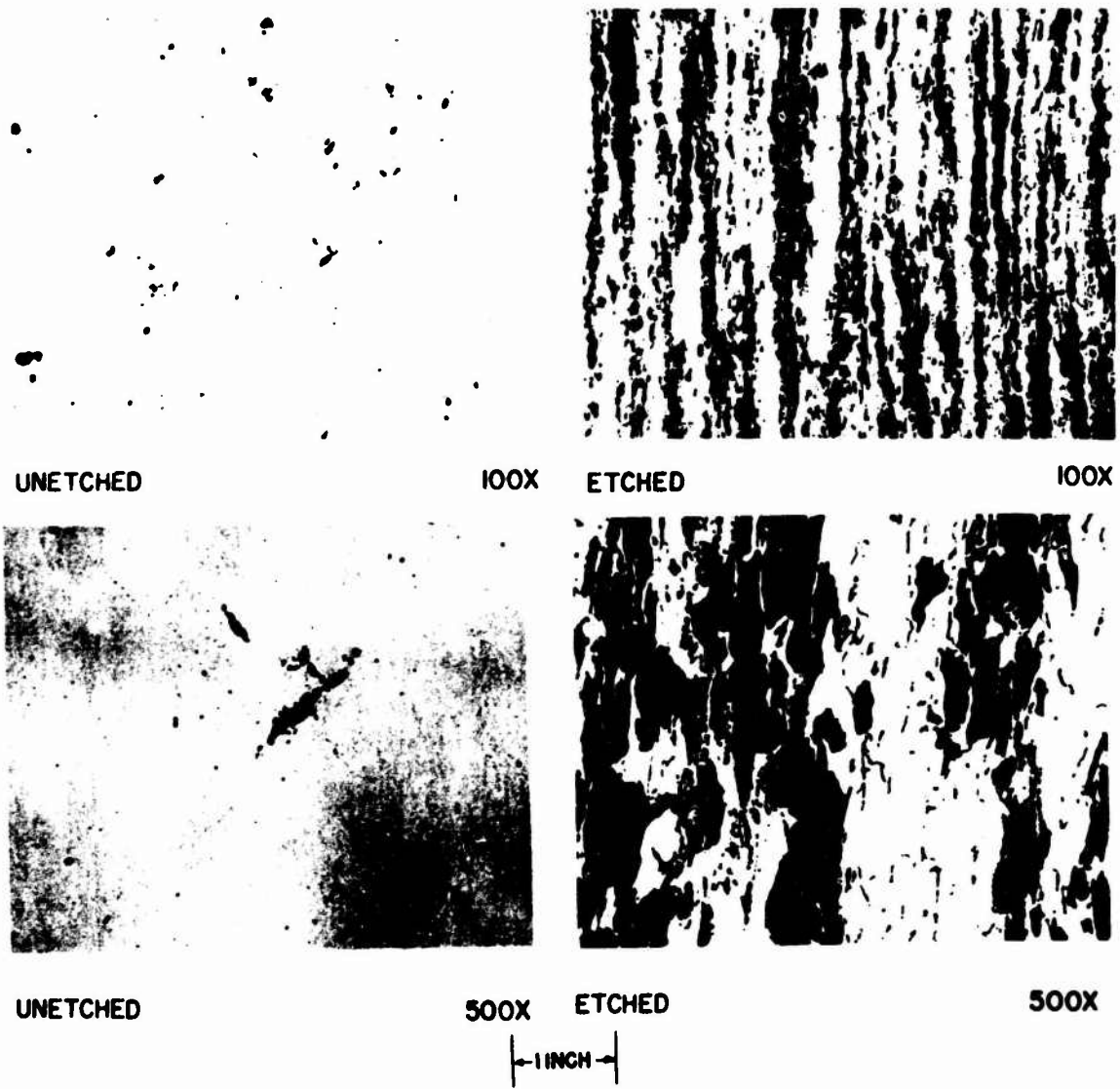
25X



FIG. 28 MICRO STRUCTURE SAE 8620

U. S. ARMY MATERIALS RESEARCH AGENCY

19-066-728/AMC-65



UNETCHED

100X

ETCHED

100X



UNETCHED

500X

ETCHED

500X



FIG. 29

MICRO STRUCTURE SAE 8620

SPEC. BRS-12

U. S. ARMY MATERIALS RESEARCH AGENCY

19-066-742/AMC-65

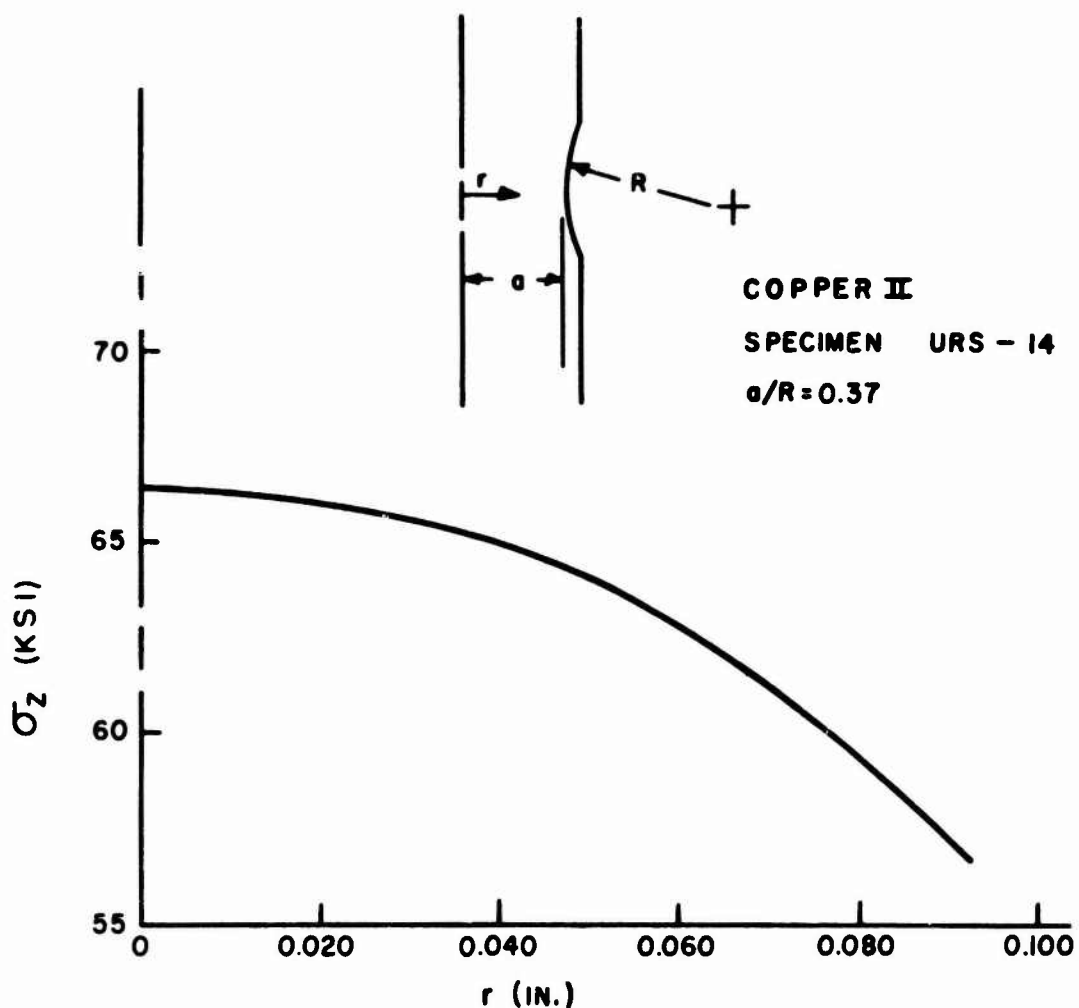
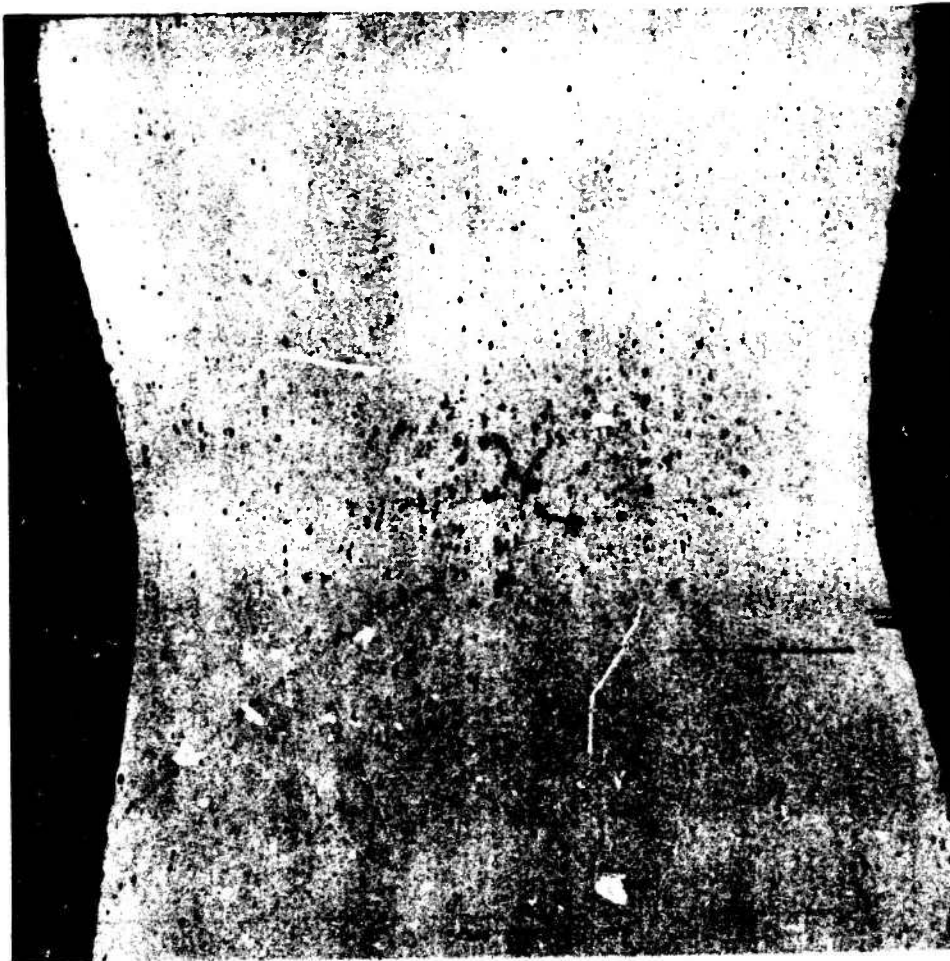


Fig. 30. LONGITUDINAL STRESS DISTRIBUTION AT INCIPIENT FRACTURE
U. S. ARMY MATERIALS RESEARCH AGENCY

19-066-707/AMC-65



UNETCHED

SPEC. URS-11

25X

← 1 INCH →

FIG. 31

MICRO STRUCTURE

COPPER CU II

U. S. ARMY MATERIALS RESEARCH AGENCY

19-066-729/AMC-65



ETCHED

SPEC. URS-11

500X

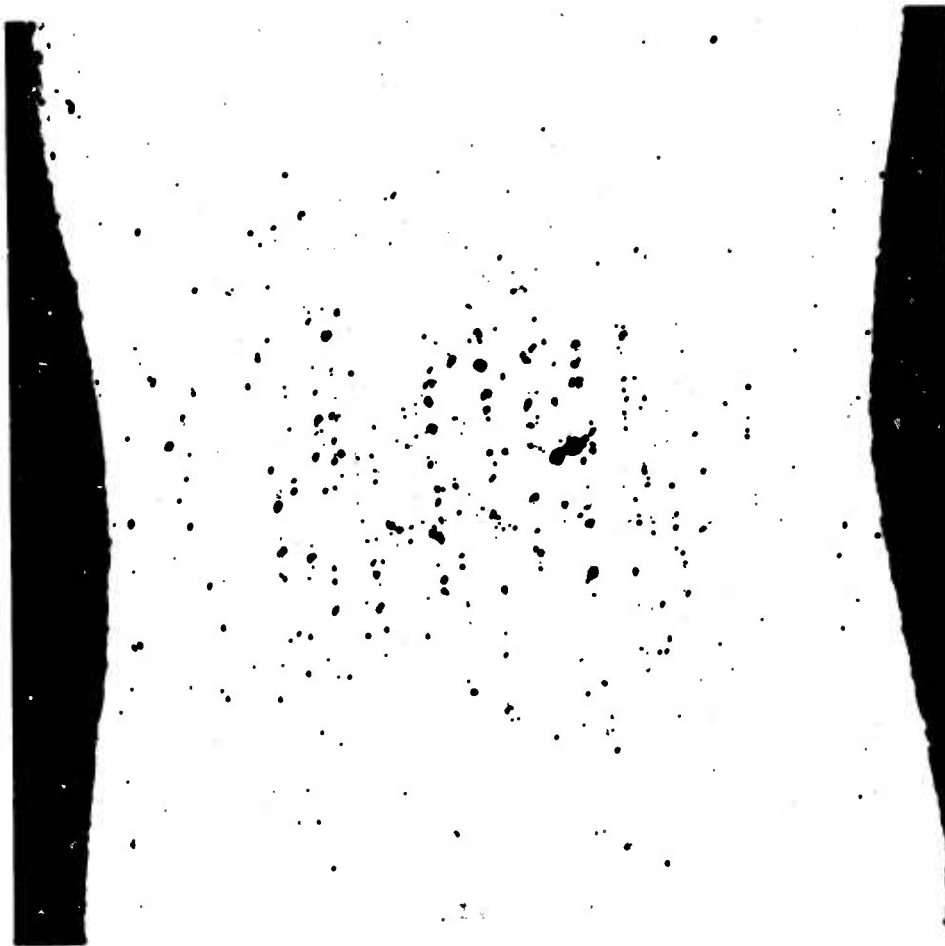
← 1 INCH →

FIG. 32

MICRO STRUCTURE COPPER CU II

U. S. ARMY MATERIALS RESEARCH AGENCY

19-066-725/AMC-65



UNETCHED

SPEC. BRS-9

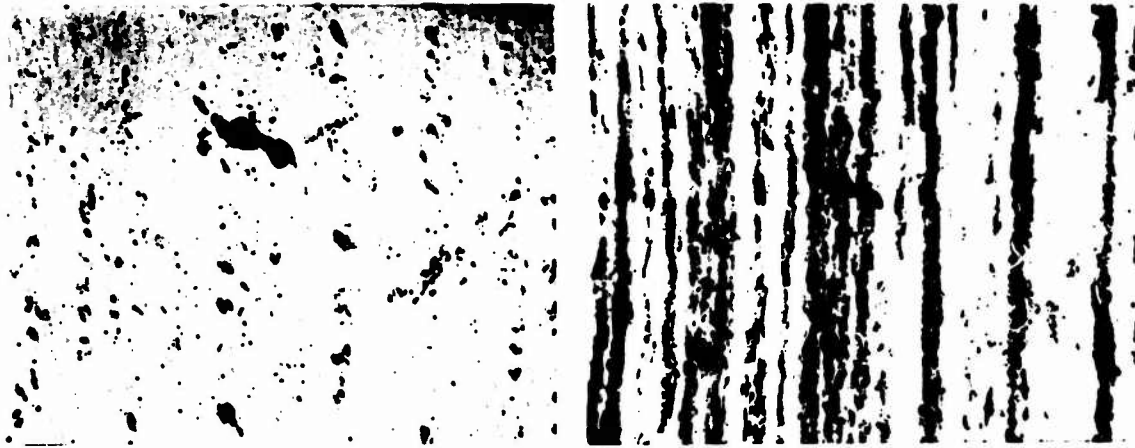
25X



FIG. 33 MICRO STRUCTURE SAE 8620

U. S. ARMY MATERIALS RESEARCH AGENCY

19-066-719/AMC-65

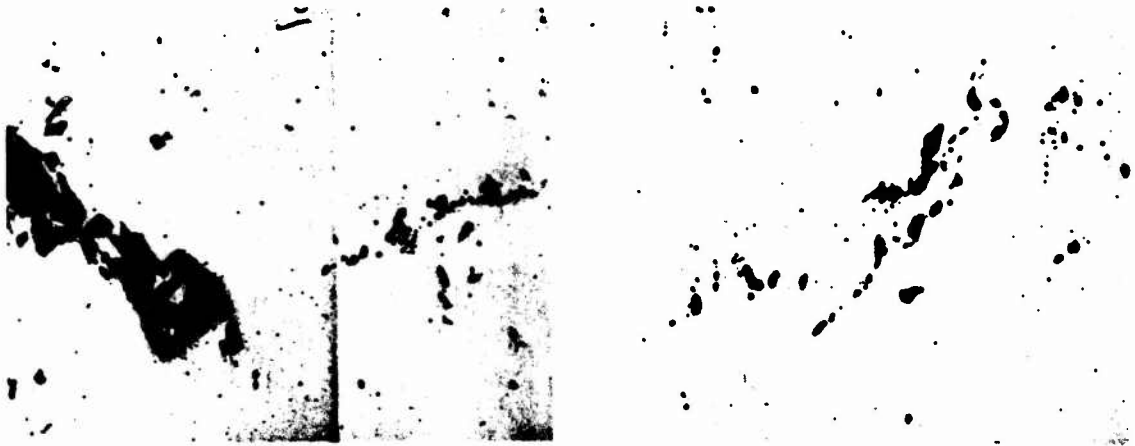


UNETCHED

100X

ETCHED

100X



UNETCHED

500X

UNETCHED

500X



FIG. 34

MICRO STRUCTURE SAE 8620 SPEC. BRS-9

U. S. ARMY MATERIALS RESEARCH AGENCY

19-066-745/AMC-65

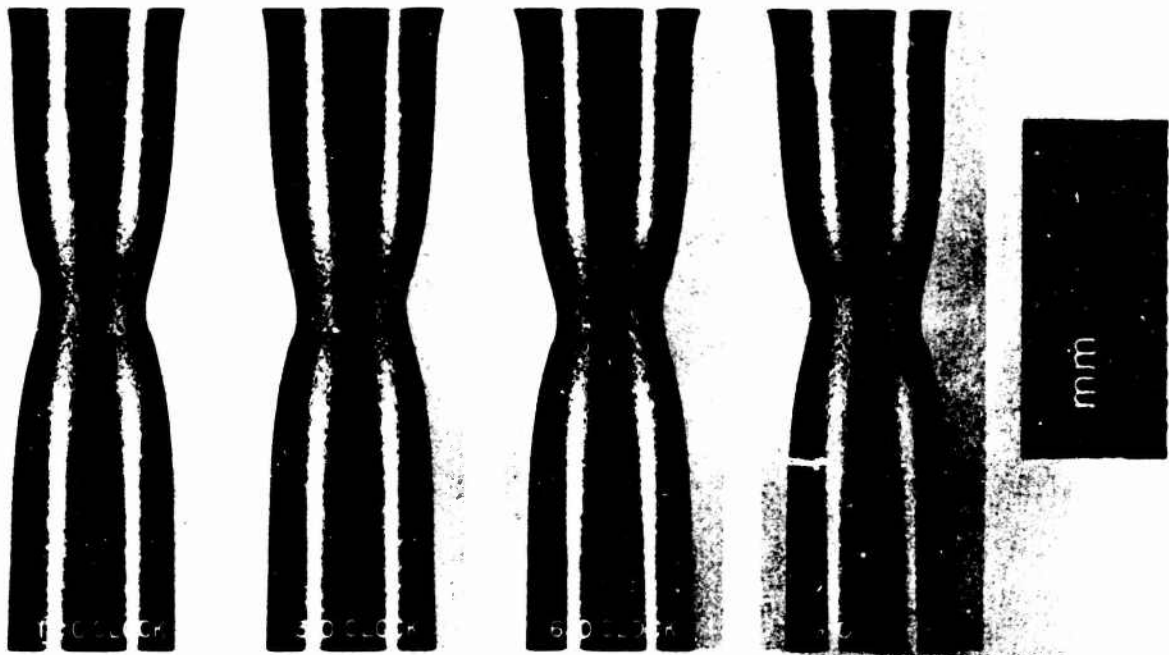


Fig. 35. EXTERIOR VIEWS OF NECKED REGION - COPPER Cu II

U. S. Army Materials Research Agency

19-066-515/AMC-65

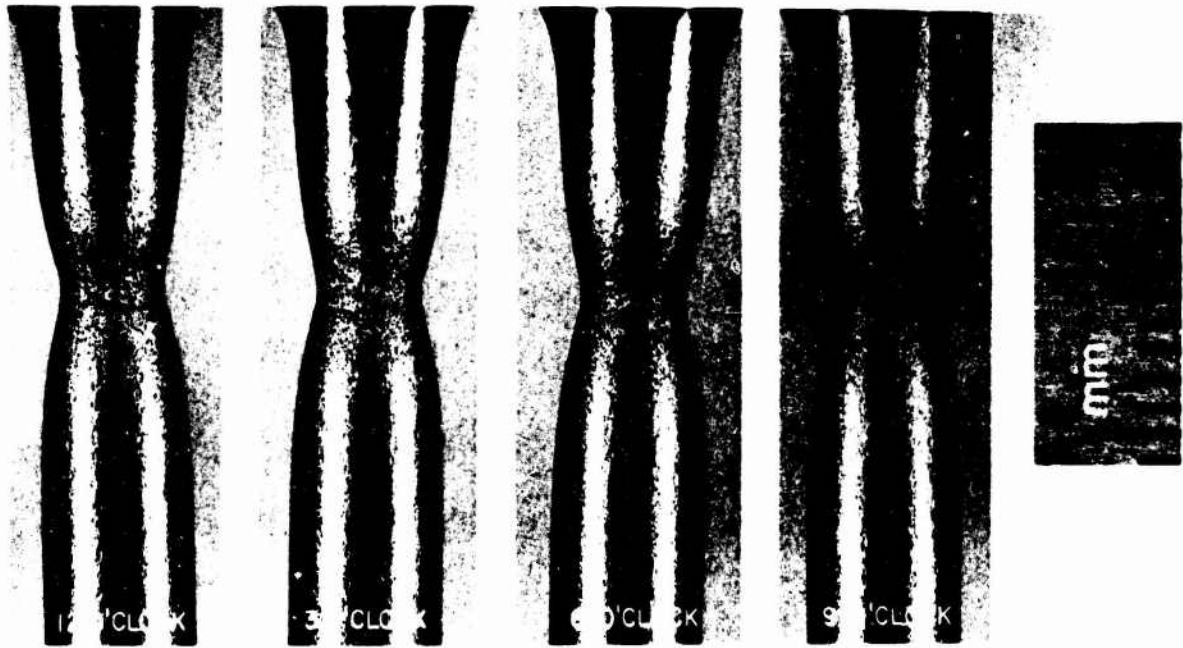


Fig. 36. EXTERIOR VIEWS OF NECKED REGION - SAE 1020

U. S. Army Materials Research Agency

19-066-516/AMC-65

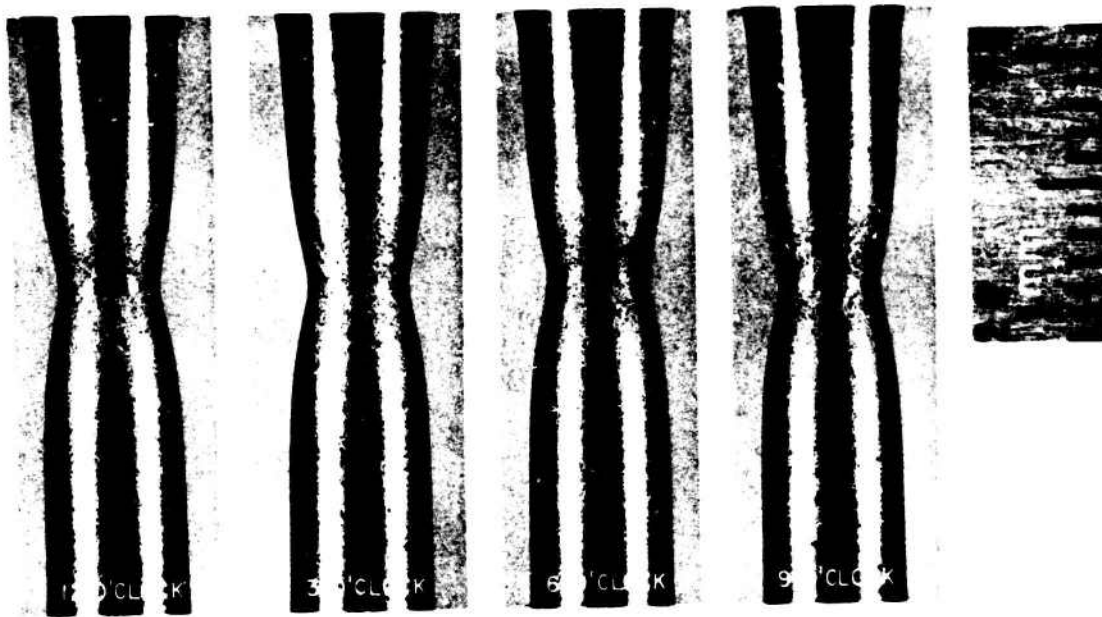


Fig. 37. EXTERIOR VIEWS OF NECKED REGION - SAE 8620

U. S. Army Materials Research Agency

19-066-517/AMC-65



19-066-722/AMC-65

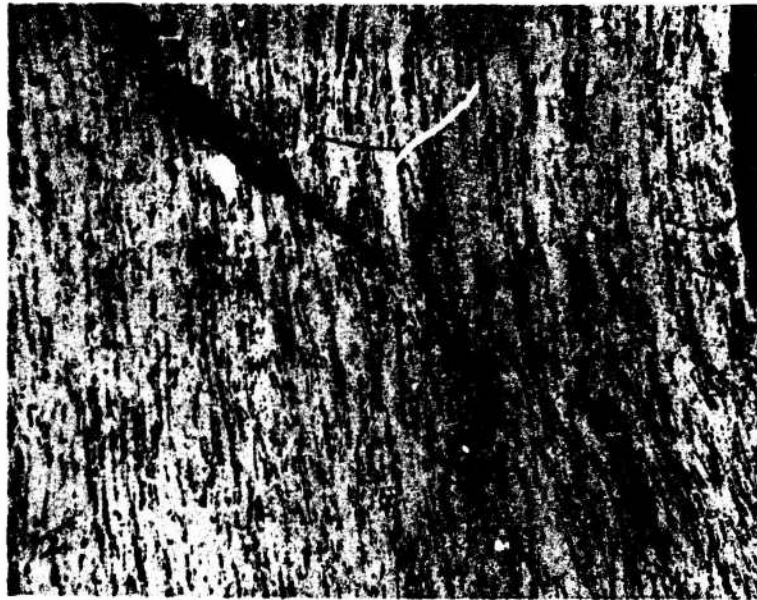
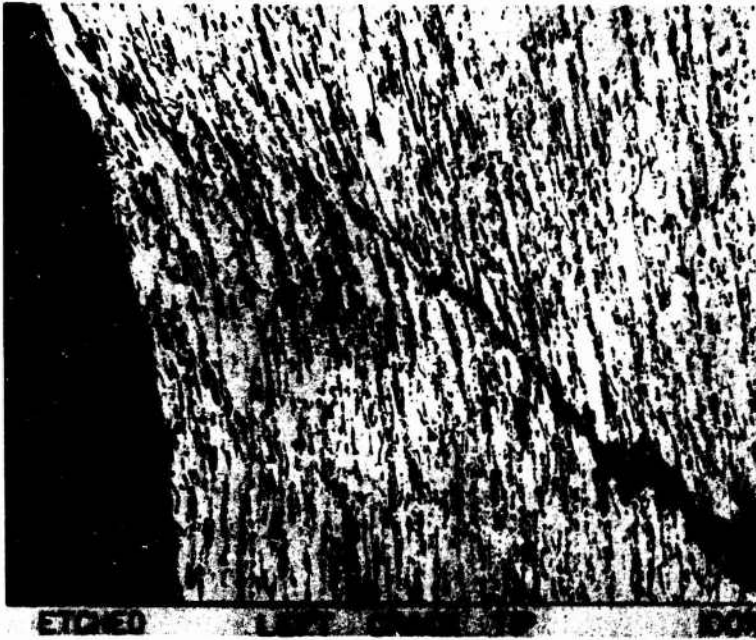
UNETCHED

SPEC. URS-9

25X



FIG. 38 MICRO STRUCTURE COPPER CU II



ETCHED

RIGHT CRACK TIP

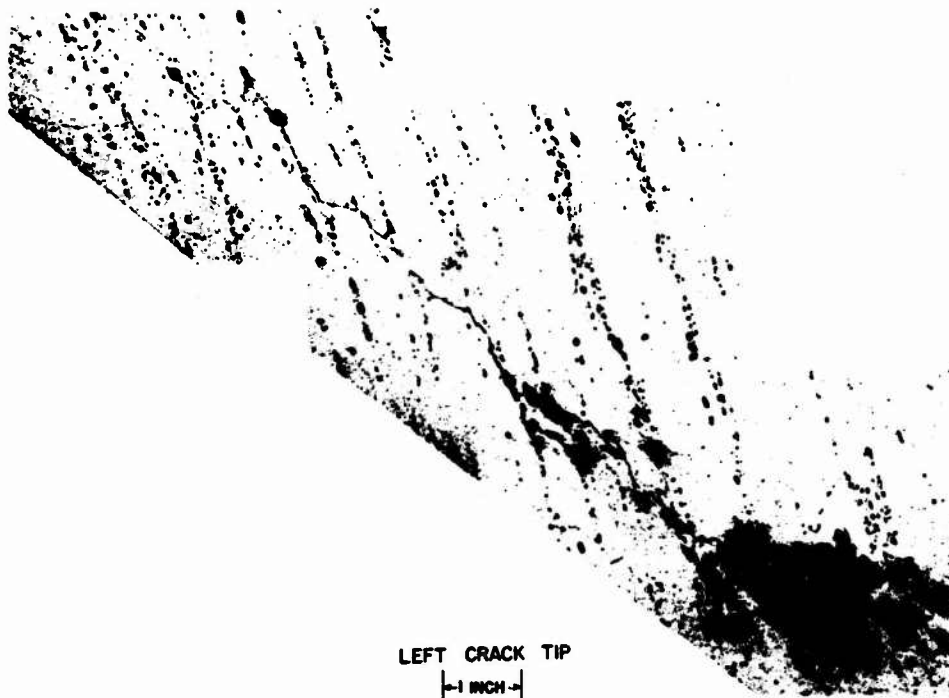
100X

← 1 INCH →

FIG. 39 MICRO STRUCTURE COPPER CU II SPEC. URS-9

U. S. ARMY MATERIALS RESEARCH AGENCY

19-066-723/AMC-65

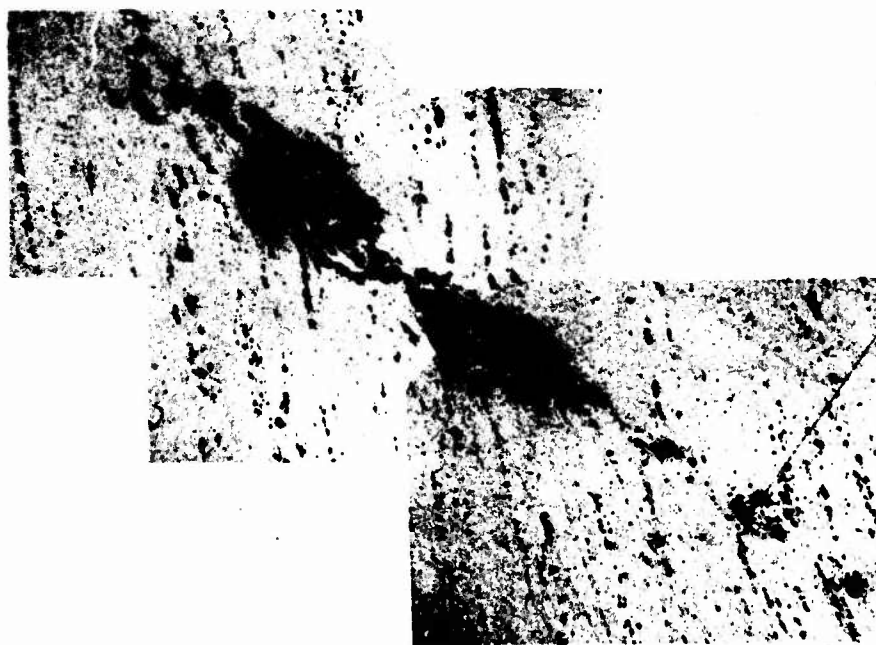


LEFT CRACK TIP
 |—1 INCH—|

19-066-743/AMC-65

UNETCHED 500X

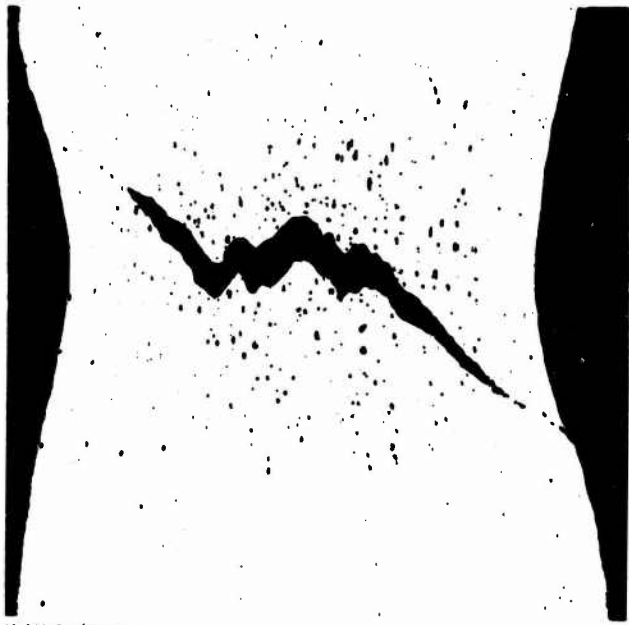
FIG. 40 MICRO STRUCTURE COPPER CU II SPEC URS-9



UNETCHED RIGHT CRACK TIP 500X
 |—1 INCH—|

19-066-734/AMC-65

FIG. 41 MICRO STRUCTURE COPPER CU II SPEC. URS-9



19-066-716/AMC-65

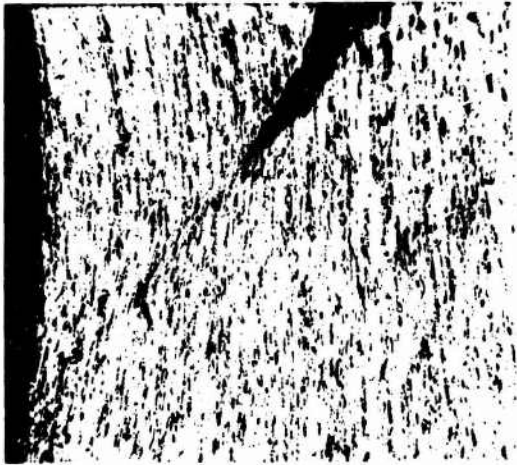
UNETCHED

SPEC. URS-7

25X



FIG. 42 MICRO STRUCTURE COPPER CU II

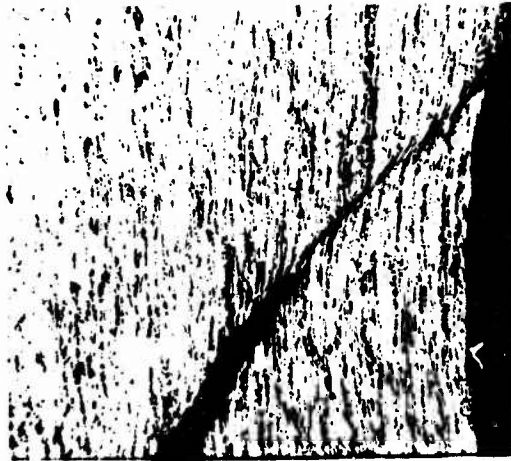


19-066-741/AMC-65

ETCHED

LEFT CRACK TIP

100X



ETCHED

RIGHT CRACK TIP

100X



FIG. 43

MICRO STRUCTURE COPPER CU II

SPEC. URS-7



ETCHED LEFT CRACK TIP 500X

|—1 INCH—|

FIG. 44 MICRO STRUCTURE COPPER CU II SPEC. URS-7

U. S. ARMY MATERIALS RESEARCH AGENCY

19-066-724/AMC-65



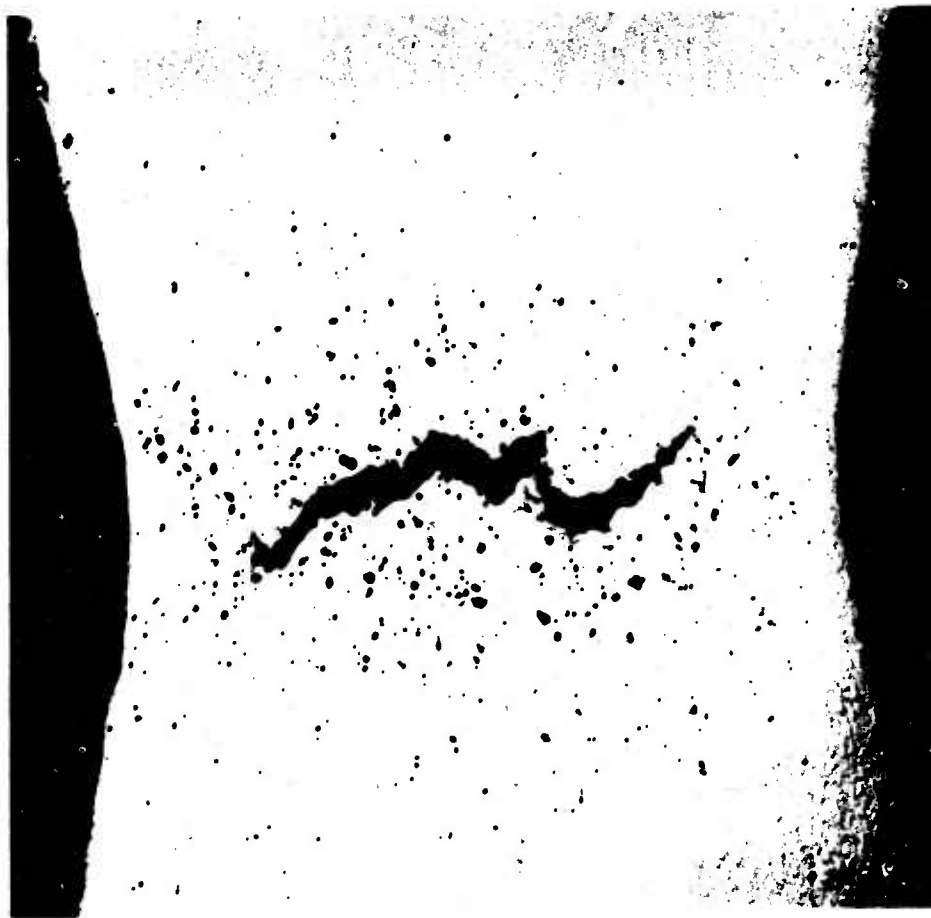
ETCHED RIGHT CRACK TIP 500X

← 1 INCH →

FIG. 45 MICRO STRUCTURE COPPER CU II SPEC. URS-7

U. S. ARMY MATERIALS RESEARCH AGENCY

19-066-713/AMC-65



UNETCHED

SPEC. GRS-12

25X



FIG. 46 MICRO STRUCTURE SAE 1020

U. S. ARMY MATERIALS RESEARCH AGENCY

19-066-711/AMC-65



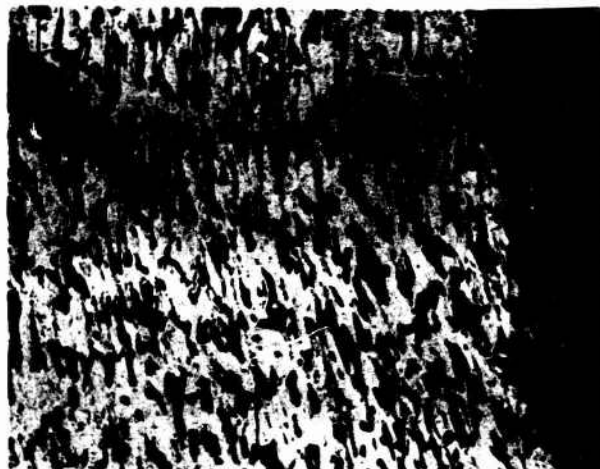
UNETCHED LEFT CRACK TIP

RIGHT CRACK TIP

100X



UNETCHED RIGHT CRACK TIP 500 X



ETCHED

RIGHT CRACK TIP

100 X



FIG. 47

MICRO STRUCTURE SAE 1020

SPEC. GRS-12

U. S. ARMY MATERIALS RESEARCH AGENCY

19-066-731/AMC-65



UNETCHED

SPEC. GRS-10

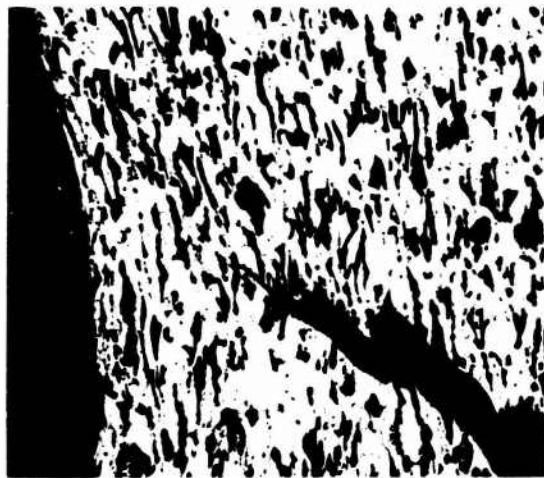
25X



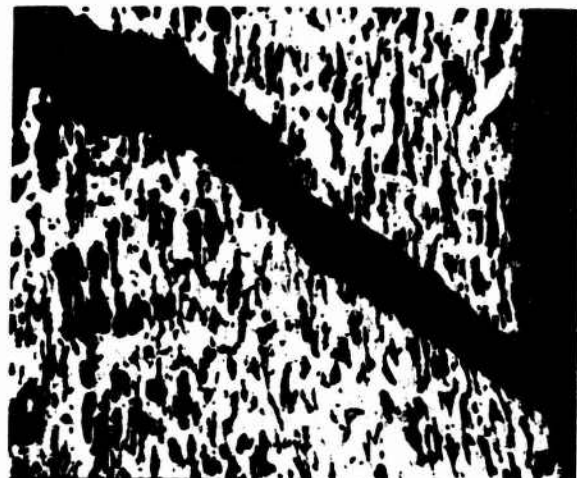
FIG. 48 MICRO STRUCTURE SAE 1020

U. S. ARMY MATERIALS RESEARCH AGENCY

19-066-712/AMC-65



ETCHED LEFT CRACK TIP 100X



ETCHED RIGHT CRACK TIP 100X



ETCHED LEFT CRACK TIP 500X
MICRO STRUCTURE SAE 1020

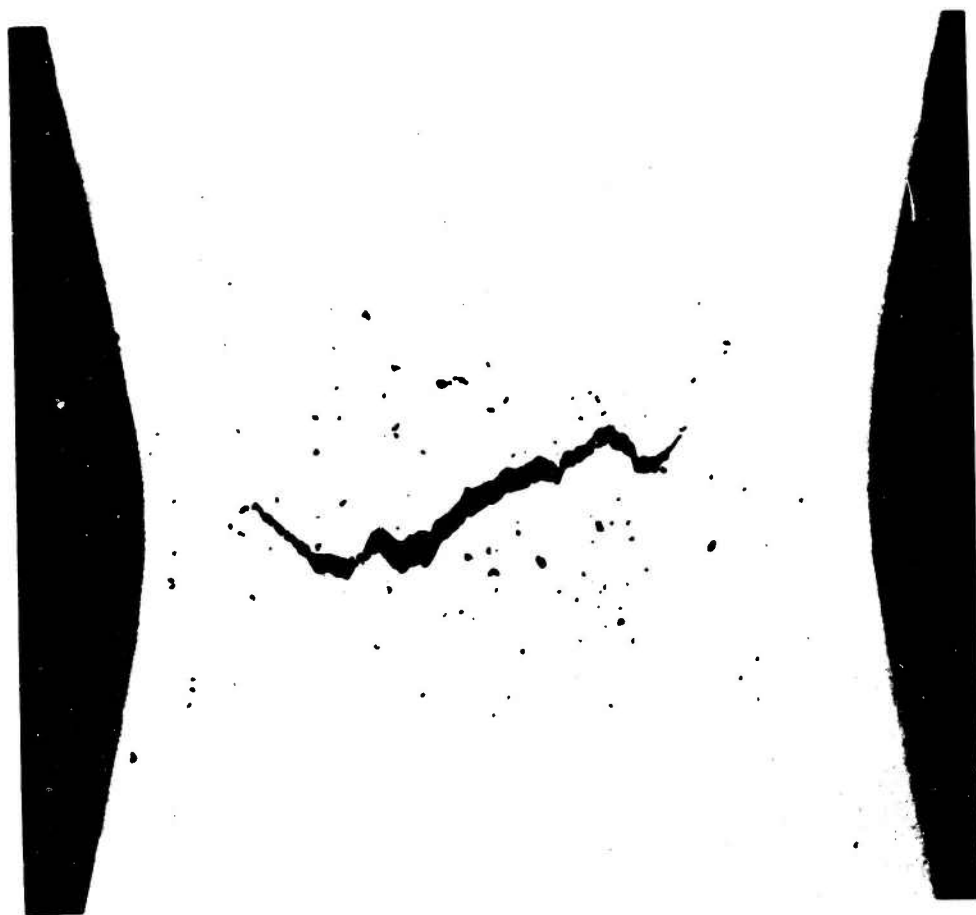


SPEC. GRS-10

FIG. 49

U. S. ARMY MATERIALS RESEARCH AGENCY

19-066-733/AMC-65



UNETCHED

SPEC. BRS-13

25X



FIG. 50 MICRO STRUCTURE SAE 8620

U. S. ARMY MATERIALS RESEARCH AGENCY

19-066-710/AMC-65



UNETCHED 500X
LEFT CRACK TIP

UNETCHED RIGHT CRACK TIP 500X

1 INCH

FIG. 51

MICRO STRUCTURE SAE 8620

SPEC. BRS-13

U. S. ARMY MATERIALS RESEARCH AGENCY

19-066-717/AMC-65

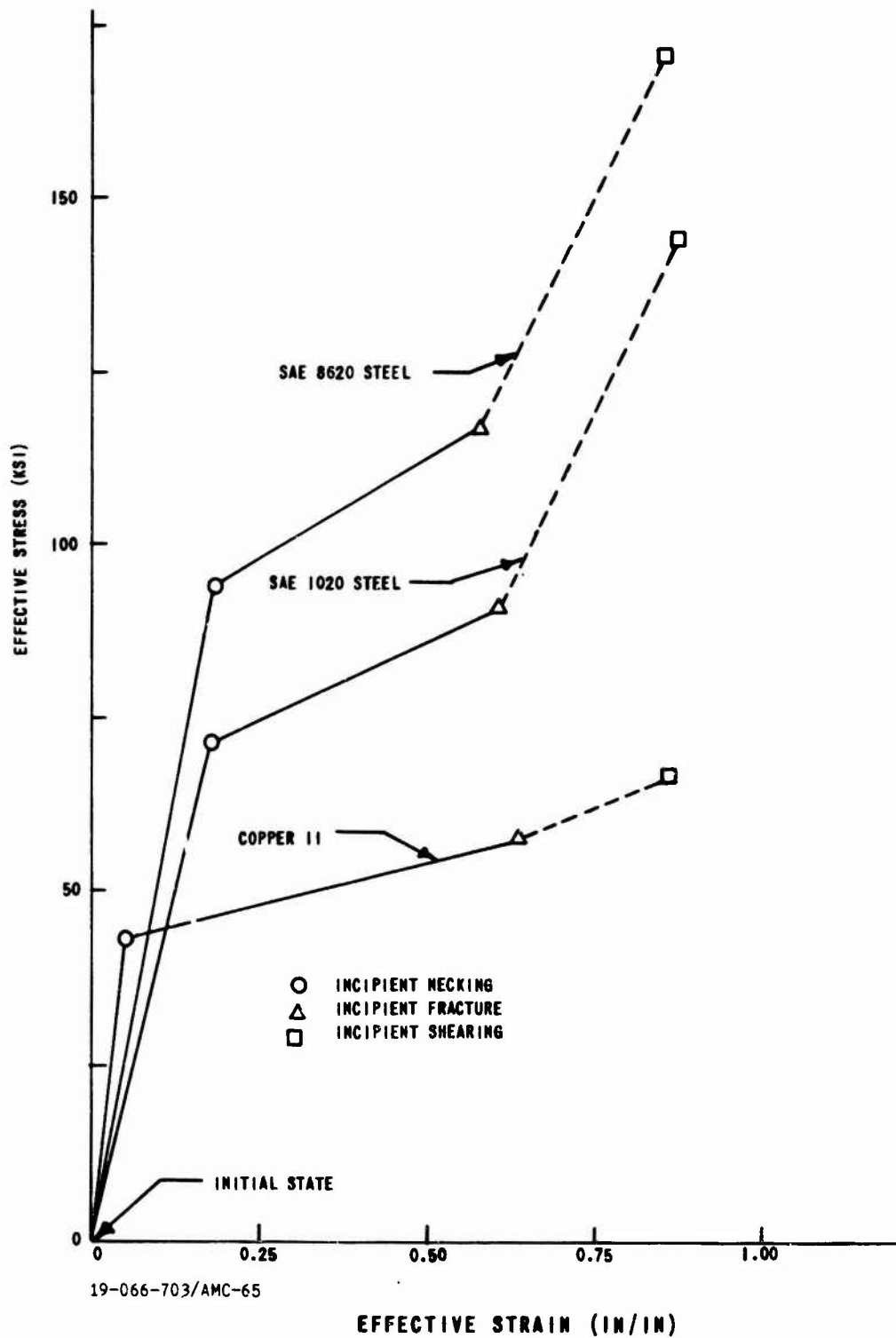


Fig. 52. EFFECTIVE STRESS-STRAIN CURVES
U. S. ARMY MATERIALS RESEARCH AGENCY